COMPARISON OF DRY AND WET COOLING: AN APPLIED RESEARCH ON A SOLAR THERMAL POWER PLANT

A THESIS SUBMITTED TO
THE BOARD OF CAMPUS GRADUATE PROGRAMS
OF
MIDDLE EAST TECHNICAL UNIVERSITY
NORTHERN CYPRUS CAMPUS

BY

ERAY TİMUR

IN PARTIAL FULLFILLMENT OF THE REQUIREMENTS
FOR
THE DEGREE OF MASTER'S OF SCIENCE
IN
SUSTAINABLE ENVIRONMENT AND ENERGY SYSTEMS

JUNE 2013

Approval of the Board of Graduate Programs

_____

Prof. Dr. Erol Taymaz

Chairperson

I certify that this thesis satisfies all the requirements as a thesis for the degree of Master of Science

_____

Asst. Prof. Dr. Ali Muhtaroğlu

Program Coordinator

This is to certify that we have read this thesis and that in our opinion it is fully adequate, in scope and quality, as a thesis for the degree of Master of Science.

_____

Asst. Prof. Dr. Eray Uzgören

Supervisor

Examining Committee Members:

Asst. Prof. Dr. Ali Muhtaroğlu, Jury Chair _____

Electrical and Electronics Engineering Program

Asst. Prof. Dr. Eray Uzgören, Jury Member _____

Mechanical Engineering Program

Assoc. Prof. Dr. Murat Sönmez, Jury Member _____

Mechanical Engineering Program

I hereby declare that all information in this document has been obtained and presented in accordance with academic rules and ethical conduct. I also declare that, as required by these rules and conduct, I have fully cited and referenced all material and results that are not original to this work.

Name, Last name:

Signature:

ABSTRACT

COMPARISON OF DRY AND WET COOLING: AN APPLIED RESEARCH ON A SOLAR THERMAL POWER PLANT

Timur, Eray

M.S., Sustainable Environment and Energy Systems

Supervisor: Asst. Prof. Dr. Eray Uzgören

June 2013, 77 pages

The present study evaluates the use of air cooled heat exchangers for an organic Rankine cycle (ORC) as part of a solar thermal power system that can produce 10-30 kWe. Overall thermal efficiency of the system under investigation relies heavily on (i) available solar thermal energy, (ii) performance of the cooling system, and (iii) power consumption due to pumps and fans within the system. For locations with good solar potential but limited water resources, it is crucial to evaluate wet cooling towers to avoid or reduce water consumption. Performance of dry cooling alternatives is limited by the dry bulb temperature rather than the wet bulb temperature, requiring more fan power to achieve the same cooling capacity. In this study, assessment of wet and dry cooling units is performed by integrating them into a small scale power plant model that uses environmental conditions (i.e. solar irradiation, ambient dry and wet bulb temperatures) as the inputs. Critical parameters include net produced power and operational costs for both wet and dry cooling units through a representative year using conditions at northern Cyprus. It is found that dry cooling unit is capable of saving water about 17 ton/MWh while it produces 6% less per annum compared to the wet cooling alternative for the representative annual weather data. Overall, dry cooling is shown to be a good solution for low altitude-humid regions, where thermal performance appears to be comparable to wet cooling while significant savings in water consumption is achieved.

Keywords: Air cooled heat exchanger, Dry cooling, Wet cooling, Organic Rankine cycle, Solar thermal

ÖZ

KURU VE SULU SOĞUTMANIN KARŞILAŞTIRMASI: BİR TERMAL GÜNEŞ SANTRALİNDE UYGULAMALI BİR ÇALIŞMA

Timur, Eray

Yüksek Lisans, Sürdürülebilir Enerji ve Çevre Sistemleri

Tez Yöneticisi: Yrd. Doç. Dr. Eray Uzgören

Haziran 2013, 77 sayfa

Bu çalışmada, 10-30 kW kapasiteli termal güneş enerjisi ile çalışan bir organik Rankine çevriminin (ORC) kuru soğutma sistemleri ile uygulanabilirliği incelenmektedir. Bu tip elektrik santrallerinin enerji verimi temel olarak; (i) güneş enerjisi yoğunluğu, (ii) soğutma sisteminin performansı ve (iii) pompa ve fanların tükettiği güç bileşenleri ile belirlenmektedir. Güneş kaynaklı enerji üretim potansiyeli yüksek olan fakat su kaynaklarının sınırlı olduğu bölgelerde, su tüketimini elimine etmek veya azaltmak adına ıslak ve kuru soğutma kulelerinin kullanımının değerlendirilmesi, sürdürülebilir enerji üretimi için gereklidir. Bu çalışmada, ıslak ve kuru soğutma birimleri için geliştirilen sayısal modeller ile küçük ölçekli bir enerji santrali modeli birleştirilerek, değişen çevre koşullarına göre (ışınım, kuru ve ıslak termometre sıcaklıkları) soğutma sistemlerinin Güneş enerjisi potansiyeli yüksek olan Kıbrıs için uygulanabilirliğini incelemektedir. Kıbrıs'ın kuzeyinde bulunan bir bölge için temsili yıl süresince değişen hava koşulları göz önüne alınmış ve üretilen net güç ve işletme maliyeti hesaplanmıştır. Temsili yılın hava şartları için, kuru soğutma ünitesinin, ıslak soğutma ünitesine kıyasla yıllık %6 daha az güç üretirken, 17 ton/MWh sudan tasarruf edebileceği bulunmuştur. Sonuç olarak, kuru soğutma ünitelerinin alçak rakıma sahip nemli bölgeler için iyi bir çözüm olduğu gösterilmiş ve kuru soğutma sistemleri ıslak soğutma sistemlerinin yerine kullanıldığında güç üretiminden çok kaybetmeden, su tüketiminden yüksek kazanç sağlamanın mümkün olduğu bulunmuştur.

Anahtar Kelimeler: Hava soğutmalı ısı dönüştürücü, Kuru soğutma, Organik Rankine çevrimi, Termal güneş enerjisi, Sulu soğutma

TABLE OF CONTENTS

LIST OF TABLES

LIST OF FIGURES

LIST OF SYMBOLS

Nomenclature

a Surface area per unit volume (m^2/m^3)

A_i Cross-sectional area of one tube (m^2)

A_{min} Minimum free-flow area (m^2)

A_{fr} Frontal area; Face area of the fill (m^2)

B Blowdown loss ($kg/hour$)

c_p Specific heat at constant pressure (kJ/kgK)

C Heat capacity of the stream (kJ/K)

C_{min} Minimum of C_a and C_w (kJ/K)

C_{max} Maximum of C_a and C_w (kJ/K)

C^* Heat capacity rate ratio, C_{min}/C_{max}

d_e Fin tip diameter (m)

d_i Inside diameter (m)

d_o Outside diameter (m)

D Drift loss ($kg/hour$)

E Evaporation loss ($kg/hour$)

h Specific enthalpy of moist air per unit mass of dry air (kJ/kg)

h_{gw} Specific enthalpy of water vapor at T_w (kJ/kg)

h_{sw} Specific enthalpy of saturated moist air at T_w (kJ/kg)

H Convective heat transfer coefficient ($W/m^2 \cdot K$)

H_d Mass transfer coefficient ($kg/m^2 \cdot s$)

k Thermal conductivity ($W/m^2 \cdot K$)

L Effective length of tubes (m)

$\dot{m}_a$ Air mass flow rate through the face area (kg/s)

$\dot{m}_w$ Mass flow rate of the water (kg/s)

n_p Number of passes (-)

n_t Number of tubes (-)

P_B Barometric pressure (Pa)

P_f Fin pitch (m)

P_l Longitudinal pitch (m)

P_t Transversal pitch (m)

P_v Vapor pressure (Pa)

ΔP_{loss} Pressure loss [Pa]

$\dot{Q}$ Heat rate (W)

T Dry bulb temperature (K)

T_{wb} Wet bulb temperature (K)

u_∞ Inlet face velocity (m/s)

u_{max} Velocity of the incoming air at the minimum surface area (m/s)

U Overall heat transfer coefficient ($W/m^2 \cdot K$)

$\dot{W}$ Power [W]

Greek letters

α	Heat transfer area/Total volume (m^2/m^3)
δ	Fin thickness (m)
ε	Heat exchanger effectiveness (-)
η	Efficiency (-)
σ	Ratio of the free flow area to frontal area, A_{min}/A_{fr}
μ	Dynamic viscosity ($Pa \cdot s$)
π_c	Cycles of concentration (-)
ρ	Density of the fluid (kg/m^3)
φ	Relative humidity (-)
ω	Humidity ratio ($kg.kg^{-1}$)
ω_{sw}	Humidity ratio of saturated moist air at T_w ($kg.kg^{-1}$)

Dimensionless symbols

j	Colburn modulus
Le_f	Lewis factor
N	Number of transfer units (NTU)
Nu	Nusselt number
Pr	Prandtl number
Re	Reynolds number
St	Stanton number

Subscripts

1	Inlet
2	Outlet
a	Air; Air side
$base$	Base surface
B	Barometric
Cu	Copper
enh	Enhanced surface
f	Fin
fr	Frontal
h	Hot fluid
i	Inside; Inner
f	Fin
max	Maximum
min	Minimum
o	Outer
p	Pass
r	Root
ref	Refrigerant
rev	Reversible
sw	Saturated moist air

V	Vapor
w	Water; Water side
wb	Wet bulb

CHAPTER 1

INTRODUCTION

Diminishing supplies of fossil fuels and their adverse impacts on environment have accelerated the research on clean and sustainable power production alternatives. Among the alternatives of renewable energy resources, concentrating solar power systems (CSP) are increasing. CSP market has already reached over 2000 MW globally by July, 2012 [1]. CSP systems are being offered not only at large scales but also at small scales as affordable energy solutions to small communities located away from the power grid. Suitable small-scale systems usually operate at low temperatures and utilize organic Rankine cycles to produce around 10-100 kW power.

Rankine cycle is by far the most widespread way of power production, meeting roughly 80% percent of electricity consumption in the world [2]. Thermal efficiency of a Rankine cycle is strongly linked to the heat rejected from the system, as Equation (1) shows:

$$\eta_{max} = 1 - \frac{Q_{rejected}}{Q_{input}} \quad (1)$$

$$\left(\frac{Q_{rejected}}{Q_{input}}\right)_{rev} = \frac{T_{low}}{T_{hot}} \quad (2)$$

Equation (1), together with the second law (2), points out that either lowering cold reservoir's temperature (T_{low}) or increasing hot reservoir's temperature (T_{hot}) can result in higher cycle efficiency.

Organic Rankine cycles (ORC) are similar to traditional Rankine cycles except that they utilize refrigerants instead of steam as their working fluid, so that they can operate between lower temperature reservoirs, yielding lower efficiencies. Because of this reason, they attracted the attention of many researchers, who are interested in investigating possible opportunities

to produce power through low-grade heat sources, such as waste heat and geothermal energy.

Solar based ORC applications require the region to have adequate solar irradiation in order to be able to operate independently. However, regions with good direct solar potential have high ambient temperature, which has an adverse effect on heat rejection. In fact, water resources of such regions are usually limited and relying on a wet cooling tower can weaken the sustainable nature of the overall system. There are various types of cooling units differing in main mode of heat transfer, draft, and size etc., which can be categorized as:

- Once-through cooling
- Wet cooling
- Dry cooling

Currently, most of the power plants around the world utilize water cooling, i.e. once-through cooling or wet cooling. In once-through cooling, thermal energy is discharged directly into a large body of water such as sea, lake etc. Although being effective and inexpensive, this method has been reported as having detrimental impacts on aquatic life, coastal waters, estuaries and bays [3]. In some regions, there are even efforts to decommission the existing facilities [4]. In the future, once-through cooling can be prone to stricter regulatory limitations due to high environmental footprint.

In wet cooling, heat is discharged to air by the water circulating in a closed cycle. This method has been quite widespread since water has been considered as cheap and abundant. However, considering their main mode of heat dissipation is by mass transfer, wet cooling towers consume huge amount of water by evaporation. In places with high solar energy potential, traditional method of wet cooling can be infeasible as these regions usually have limited water resources.

Dry cooling systems constitute the main alternatives to water-based cooling systems. Such systems are labeled as 'dry', because there is no need for make-up water. Actually, up to 90-95% of the water can be saved with dry cooling with sacrifice of cooling efficiency especially on hot days.

The present study focuses on the comparison of wet and dry cooling for conditions at Northern Cyprus. The system under consideration is a micro-scaled CSP system where cooling is achieved by means of a wet-cooling tower already in place.

System Description

Solar thermal system installed at Middle East Technical University, Northern Cyprus Campus (METU NCC) is constructed in collaboration with the SOLITEM Group which is an international renewable energy company. The initial design was intended to reduce cost while improving reliability. There are three main components: Parabolic trough solar collectors as the heat source, an Organic Rankine Cycle (ORC) for electricity generation, a cooling tower for heat rejection. The layout of the whole system is illustrated in Figure 1.

Parabolic trough collectors (PTCs) with non-evacuated covers target to carry thermal energy at a lower temperature range, to make the system cheap with little maintenance. Tubes of the collectors on hand contain air resulting in poor insulation compared to more costly evacuated tubes [5]. Pressurized water gets heated through direct irradiation as it circulates through PTCs. Installed at a 540 m^2 area, the total surface area of the collectors is 216 m^2.

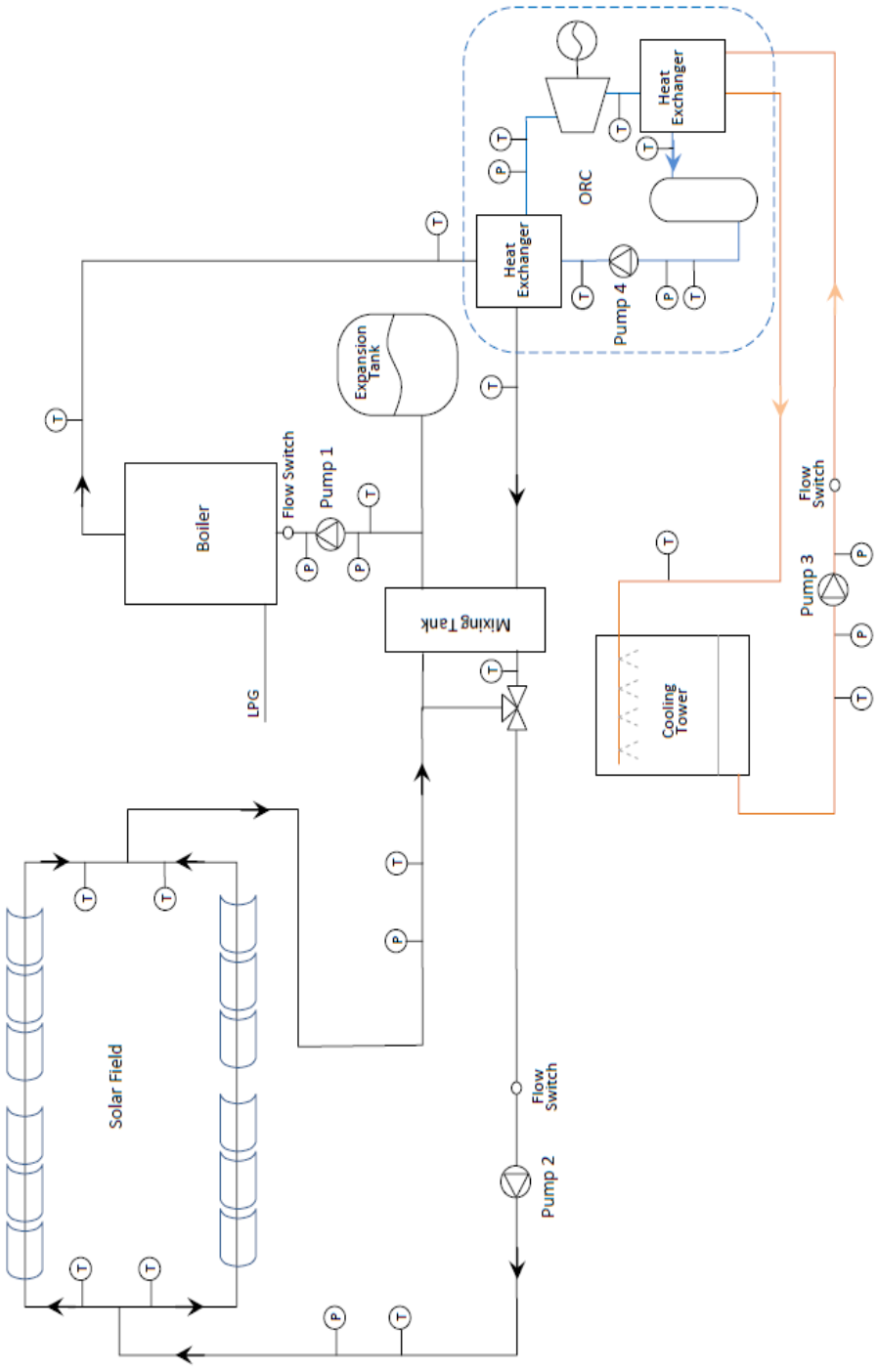

Figure 1: The Plant Overview

The second component, Organic Rankine cycle (ORC), is primarily a Rankine cycle which utilize a special fluid instead of water and is primarily designed for low grade heat resources such as waste heat, geothermal and solar [6]. Working fluid of the ORC is a refrigerant, R245fa, produced by Genetron®. With the boiling temperature of 15°C at 1 atm, it is a good choice for the small scale solar thermal systems.

The third component is a counterflow cooling tower. This unit utilizes water to condense refrigerant through a heat exchanger at the turbine exit. As the enthalpy of refrigerant decreases, energy is discharged to water; which is then pumped to the cooling tower, where water transfers heat to the environment by mainly mass transfer and convective heat transfer.

Dry and wet cooling

Dry and wet cooling systems discharge heat to ambient environment via different mechanisms. Wet cooling systems reject heat mainly by evaporative cooling. On the other hand, main mode of heat transfer is convection for dry cooling.

Cooling capabilities of both configurations are limited by ambient conditions. Dry bulb temperature affects dry cooling systems performance and wet bulb temperature for wet cooling systems. While high temperatures reduce efficiency for both, high humidity ratio decreases the performance of wet cooling towers.

Level of the respective temperature (dry bulb temperature for dry cooling and wet bulb temperature for wet cooling) influences the condenser temperature and hence the back-pressure of the turbine and efficiency. This is an advantage for wet cooling units as the wet bulb temperature is always less than or equal to the dry bulb temperature. However, the tradeoff for wet cooling, i.e. makeup water requirements, needs to be taken into account to achieve better sustainability.

Water consumption of a cooling tower is the sum of blowdown, evaporation and drift losses, which is equal to makeup water requirement for a particular cooling tower. Evaporative and blowdown losses constitute the major portion. Evaporative losses refer to the amount transferred from circulating water to the air flow while blowdown losses are related to the cooling tower circulating water periodically discharged to ensure the percentage of dissolved solids in cooling water is kept at certain levels. Drift loss, related to the liquid droplets being carried out by the air flow, does not constitute a significant portion and they can even be minimized by the use of drift eliminators, which can be as small as 0.002% of water circulation rate [7]. The relationship between them is illustrated in Figure 2.

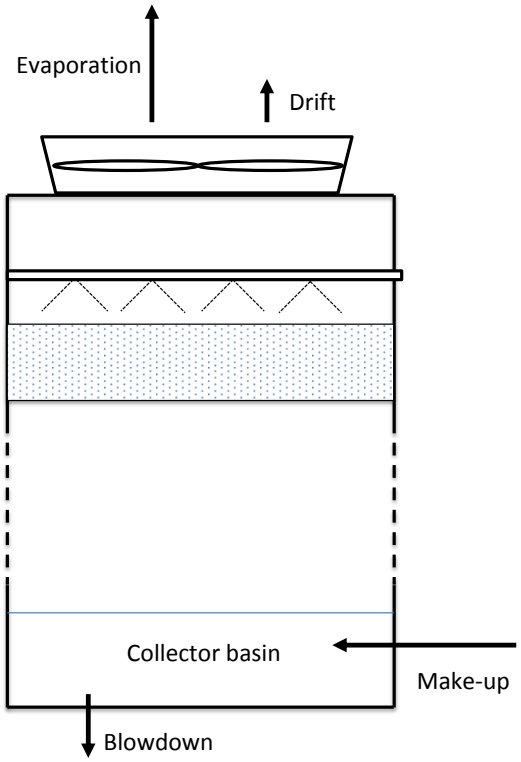

Figure 2: Water mass balance for cooling towers

Dry and wet cooling systems can be categorized into two types by the way air is passing through the cooling unit: natural draft and mechanical draft. Natural draft systems require the use of large chimneys to utilize natural

buoyancy forces driven by the pressure difference between bottom and top of the tower. These types of systems are more suitable to utility scale power plants. Mechanical draft systems, on the other hand, employ fans to maintain air flow. These systems are categorized as either forced or induced draft depending on where fans are mounted. In the former, fans compress air and fans suck air for induced draft.

Dry cooling systems can also be classified as direct and indirect cooling. In direct dry cooling, i.e. air cooled condensers, fans blow air over the bundles of finned-tubes, where heat rejection occurs and turbine exhaust steam condenses. Matimba power plant in South Africa is an example of this type [8]. Schematic of a direct dry cooling unit is shown in Figure 3.

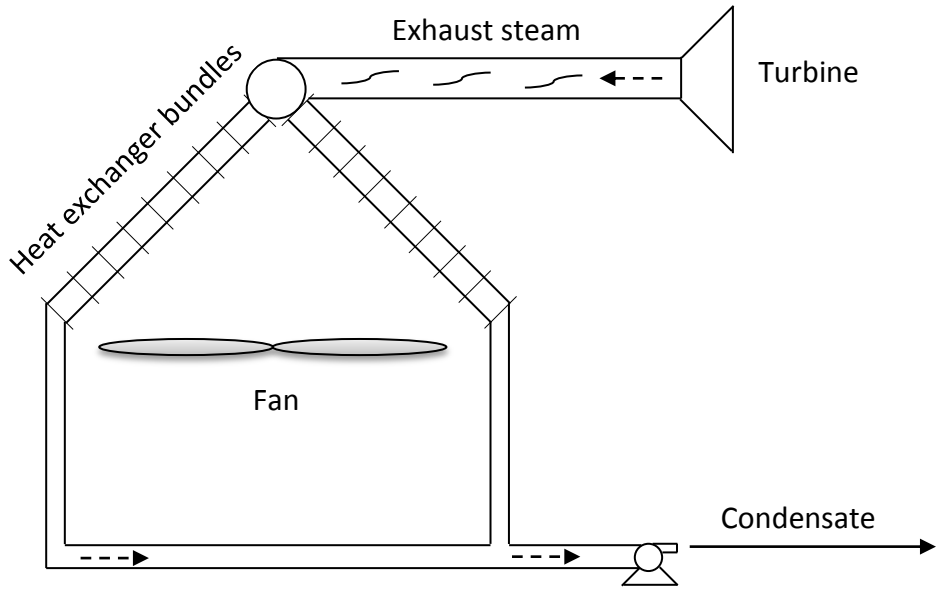

Figure 3: Direct type dry cooling

In indirect dry cooling, water is the primary coolant that removes heat from the system of interest while air is the secondary cooling medium to remove heat from water flowing in a closed cycle. A real life example of this type is Grootvlei power plant in South Africa [9]. Figure 4 illustrates an example of a mechanical draft indirect dry cooling unit.

Since the first appearance of a dry cooling unit of substantial capacity at a power plant in 1962 at Rugeley (U.K.) [10], so much attention has been paid to enhance the performance of this emerging technology.

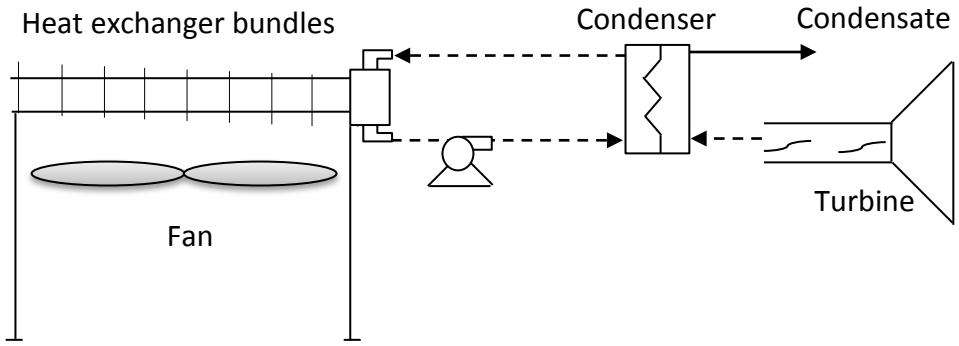

Figure 4: Indirect type dry cooling

Previous studies on dry cooling unit mainly focuses on restraining the detrimental effects of crosswind [3] [11] [12] [13], inlet flow losses [14] [15] [16], and ways to alleviate performance penalties attached to high temperatures [17]. Regarding the studies considering crosswind, Goodarzi [3] proposed a new stack configuration instead of wind breakers, which is previously already studied by various researchers. Zhai and Fu [11] investigated optimal scale of wind-break walls to reduce losses in cooling efficiency under cross-wind. Stinnes and Backström [12] investigated the adverse impacts of cross-flow considering the flow pattern through air-cooled heat exchanger fans. LiJun et al. [13] suggested some measures to reduce the adverse impacts of natural wind by creating physical and mathematical models of dry cooling units and conduction CFD simulation.

The issue of inlet flow losses has been another focus of researchers. Meyer and Kröger [14] carried out an experimental study investigating the relationship between air-cooled heat exchanger geometry and inlet air flow losses. Studies [15] and [16] examined the effect of platform height on the performance of forced-draught air-cooled heat exchangers.

Gadhamshetty et al. [17] proposed a new method, precooling inflow air utilizing a chilled-water thermal energy storage system, to reduce performance penalties during times of high ambient temperatures.

Despite the enthusiasm to further explore dry cooling units, studies focusing on the comparison of dry and wet cooling systems under changing ambient conditions are limited. Some examples of such studies include [4] [8] [18] [19] [20] which performed comparisons with a direct type air cooled condenser (ACC) dry cooling unit for large scale power plants while the present study focuses on an indirect type air cooled heat exchanger (ACHE) for dry cooling at small scale.

Regarding the recent ORC related research, studies such as [21] [22] [23] [24] [25], focuses mainly on working fluids and temperature limits to optimize system performance at the design level. There are not many studies focusing on ORC's condenser and its use with a cooling unit. Sun & Li [24] have recently investigated off-design performance of an ORC for various decision variables, including air cooled condenser fan mass flow rate. Their ORC system comprised of high mass flow rates for a 5 MW power plant and they developed an optimization technique for system efficiency by adjusting the condenser's mass flow rates when available thermal energy input level changes. They also considered ambient conditions but it was limited to two different dry bulb temperature levels.

The present study focuses on the feasibility of indirect air-cooled dry cooling units for a small-scale organic Rankine cycle to replace the currently installed mechanical draft cooling wet tower for heat rejection.

Objectives and Scope of the Thesis

The main focus of the research is to investigate the differences between two technologies in terms of their influences on the overall system efficiency. Comparison is established over specific configurations for both dry and wet

cooling systems. The wet cooling system considered is inspired by the cooling tower currently installed as part of the micro-scaled CSP system, whereas the dry cooling unit is selected considering off-the-shelf heat exchanger surface to replace the present system's wet cooling tower. Selection/sizing stages of both dry and wet cooling units are established through developed steady state models. An integrated model including ORC is developed and applied to simulate both dry and wet cooling systems using a representative annual weather data for northern Cyprus. Relative operating costs, related to make-up water and fan power, are compared for both configurations.

One can find the details on selection and sizing procedure for wet cooling and dry cooling in Chapter 2 and Chapter 3 respectively. Overall, the objectives of this thesis are listed as follows:

1. Evaluation of the effects of ambient temperature and humidity ratio on the current system configuration and an alternative dry cooling system.

2. Comparison of the two configurations through simulations for varying ambient conditions.

3. Quantification of the reduction in water consumption when dry cooling case is considered.

4. Redesign of the dry cooler with a heat exchanger surface of higher effectiveness and its subsequent reevaluation.

The comparison is established by means of separate numerical models for dry and wet cooling systems with the following common scenarios;

- Same ambient conditions (i.e. temperature, humidity ratio)
- Same mass flow rate within the Organic Rankine Cycle (ORC)
- Same mass flow rate within the cooling cycle
- Hot water temperature is related to solar irradiation and considered as independent of varying ambient conditions.

The parameters of interest are:

- Outlet cold water temperature
- System work output
- Relative water consumption of three cases: wet cooling, dry cooling with base surface and dry cooling with enhanced surface
- Relative operating costs for the above three cases (water costs vs. fan power costs)

Thesis overview

In Chapter 1, basics of dry cooling and wet cooling are introduced along with the related literature, in the context of the thesis. Chapter 2 addresses fundamental principles behind wet cooling systems and proposes a numerical model utilized for sizing of cooling tower and for evaluating water consumption. Chapter 3 describes step by step sizing procedure for the dry cooling unit by effectiveness-NTU method. At the end of Chapter 3, an alternative heat transfer surface for dry cooling unit is also considered for its value. In Chapter 4, integration of the designed cooling units with the ORC is explained. In Chapter 5, simulation results are presented for both configurations. The thesis ends by detailing significant conclusions and possible future work in Chapter 6.

CHAPTER 2

ANALYSIS OF WET COOLING

The analysis of wet cooling can be considered in two main parts: Design phase and simulation phase. In the former, aim is to size a cooling tower for the predefined design conditions. In the latter, the behavior of the predefined cooling unit is observed for changing conditions.

The theory and the governing equations, on which both design and simulation phase rely on, are explained in the following sections. These are followed by the calculation of required tower volume and water consumption for design conditions reported at the selected site. The solution approach is illustrated in Figure 5. Results of the simulation phase are discussed in Chapter 5.

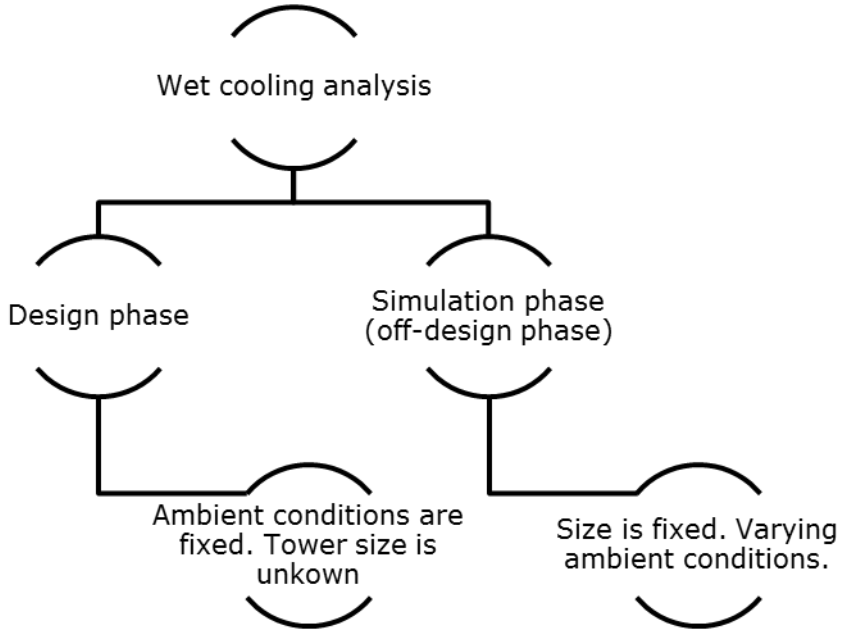

Figure 5: Wet cooling analysis

Fundamentals of wet cooling

An induced draft counter-flow cooling tower as shown in Figure 6 is considered for the analysis of wet cooling. Considering there is hot and saturated moist air at the water interface, and relatively less humid and colder air stream flowing in counter direction, mass transfer and convective heat transfer occur between streams.

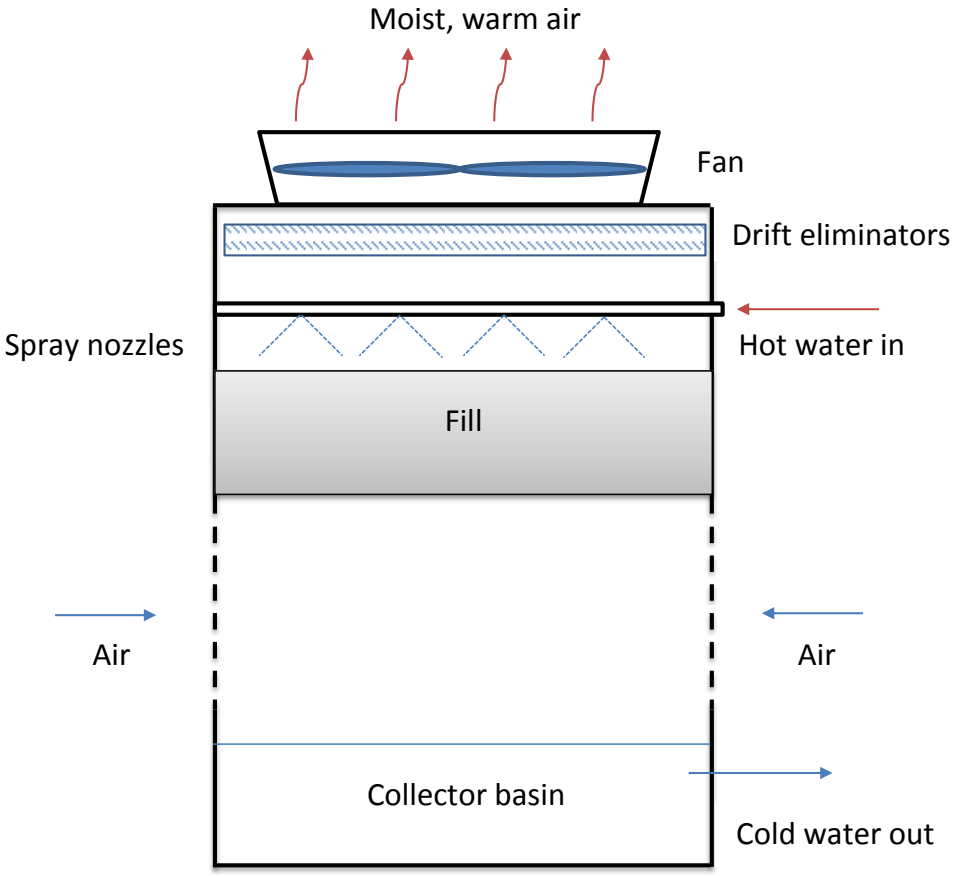

Figure 6: Induced Draft Counterflow Wet-Cooling Tower

A finite volume based analysis tool has been developed to consider mass and heat transfer between moist air and water. The approach considers dividing heat transfer surface into discrete control volumes. Change of properties in each elementary control volume is represented in Figure 7.

Control volume analysis considers following assumptions:

- water interface temperature is equal to the bulk water temperature,
- heat and mass transfer are perpendicular to the flow direction, and
- thermodynamic properties are fixed within each control volume.

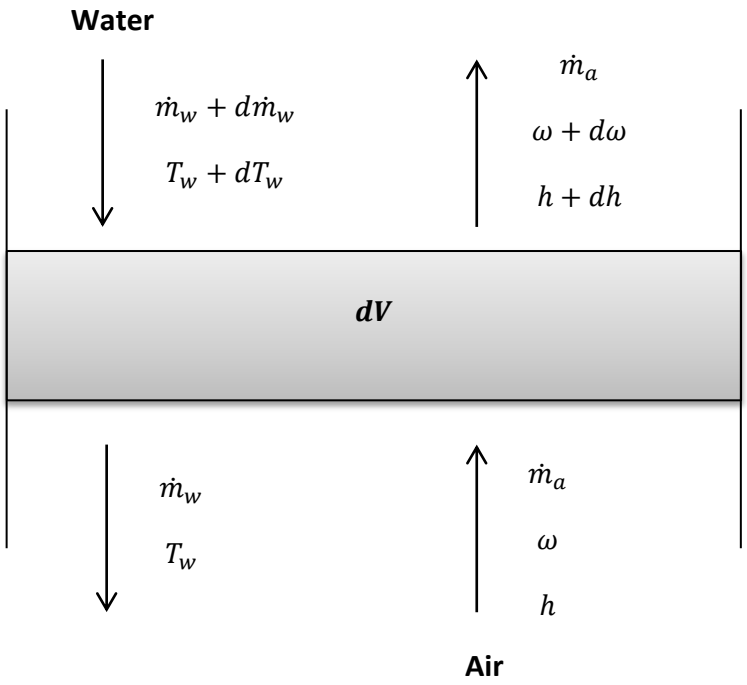

Figure 7: Property changes in differential volume

For each elementary control volume, mass and energy balance equations can then be written as:

$$\dot{m}_w + d\dot{m}_w + \dot{m}_a + \dot{m}_a\omega = \dot{m}_w + \dot{m}_a + \dot{m}_a(\omega + d\omega) \quad (3)$$

$$(\dot{m}_w + d\dot{m}_w)c_{p,w}(T_w + dT_w) + \dot{m}_a h = \dot{m}_w c_{p,w} T_w + \dot{m}_a(h + dh) \quad (4)$$

where ω represents the humidity ratio, c_p is the specific heat at constant pressure, h is the specific enthalpy, T_w is the water temperature and the subscripts, w and a, represent water and air, respectively. Eq. (3) and (4) can be manipulated into Eq. (5) to represent the change in water temperature between each control volume. Note that the term $d\dot{m}_w dT_w$ is neglected.

$$dT_w = \frac{\dot{m}_a}{\dot{m}_w c_{p,w}}(dh - c_{p,w}T_w d\omega) \tag{5}$$

Eq. (5) requires an additional relation to characterize change in enthalpy with change in humidity ratio, as given in the following equation [7]:

$$\frac{dh}{d\omega} = Le_f \frac{h_{sw} - h}{\omega_{sw} - \omega} + (h_{gw} - 2501Le_f) \tag{6}$$

where h_{gw} is the specific enthalpy of water vapor at T_w, and Le_f is the Lewis factor defined by the ratio $H_c/H_d c_{p,a}$. Saturated moist air's specific enthalpy, h_{sw}, and the humidity ratio of saturated moist air at water temperature , ω_{sw} , are calculated using the following equations:

$$\omega_{sw} = 0.622P_v/(P_B - P_v) \tag{7}$$

$$h_{sw} = (1.006 + 1.805\omega_{sw})T_w + 2501\omega_{sw} \tag{8}$$

Lewis factor is different than the Lewis number and can be approximated by the Bosnjakovic correlation as shown in Equation (7) [26].

$$Le_f = 0.865^{2/3}[(\frac{\omega_{sw} + 0.622}{\omega + 0.622} - 1) \,/\, \ln(\frac{\omega_{sw} + 0.622}{\omega + 0.622})] \tag{9}$$

Discrete forms of Eqs. (5) and (6) for a single control volume are represented by the following equations,

$$\frac{h_{i+1} - h_i}{\omega_{i+1} - \omega_i} = Le_{f,i}\frac{h_{sw,i} - h_i}{\omega_{sw,i} - \omega_i} + (h_{gw,i} - 2501Le_{f,i}) \tag{10}$$

$$T_{w,i+1} = T_{w,i} + \frac{\dot{m}_a}{\dot{m}_w\, c_{p,w,i}}((h_{i+1} - h_i) - c_{p,w,i}T_{w,i}(\omega_{i+1} - \omega_i)) \tag{11}$$

Equations (10) and (11) are utilized for calculation of volume of the fill section. They are solved by incrementing enthalpy from the bottom of the fill where air enters cooling tower at ambient conditions, which can be characterized by the dry bulb temperature, T, and the wet bulb temperature, T_{wb} (or humidity ratio, ω). As for calculation of volume, inlet and exit temperatures of water, T_{w1} and T_{w2} are known. In the first step,

properties of water and air is found for the first control volume (i=1). Once a small increment in specific enthalpy, $\Delta h = h_{i+1} - h_i$, is selected, the humidity ratio at the next control volume, ω_{i+1}, is calculated using Eq. (10). Water temperature at the next control volume, $T_{w,i+1}$, is also computed using the pre-assumed enthalpy increment and the corresponding humidity ratio change. At each step, $h_{sw,i}$ and $\omega_{sw,i}$ are updated using the new value of $T_{w,i}$. The procedure is repeated until $T_{w,i}$ is equal to T_{w1}. Finally, the corresponding fill volume is calculated accordingly. The summary of the solution procedure is illustrated in Figure 8.

Cooling tower volume

The design of the cooling tower is based on the induced draft counterflow configuration as seen in Figure 6. The main motivation behind the selection is the widespread usage of this configuration in power plants. The other reason is that hot plume recirculation is not that much of a concern as it is for forced draft configuration [9] [27]. Effect of plume recirculation is neglected in the present study/thesis.

The solar thermal power plant is in the northwestern region of Cyprus at a near sea-level coastal town. Consequently, sea level barometric pressure, i.e. 1 atm, is assumed in calculations. In addition, the design conditions data is selected for the closest region where the geographic and climatic conditions are similar and there is available design conditions data [28]. Relevant parameters are presented in Table 1.

Table 1: Design Conditions for Paphos (SI Units) REF: [28]

Country	Station	Elevation (meter)	0.4% Design Condition (°C)		1.0% Design Condition (°C)		2.0% Design Condition (°C)	
			Dry Bulb	Wet Bulb	Dry Bulb	Wet Bulb	Dry Bulb	Wet Bulb
Cyprus	Paphos	8	31.1	24.4	30	24.4	29.4	24.4

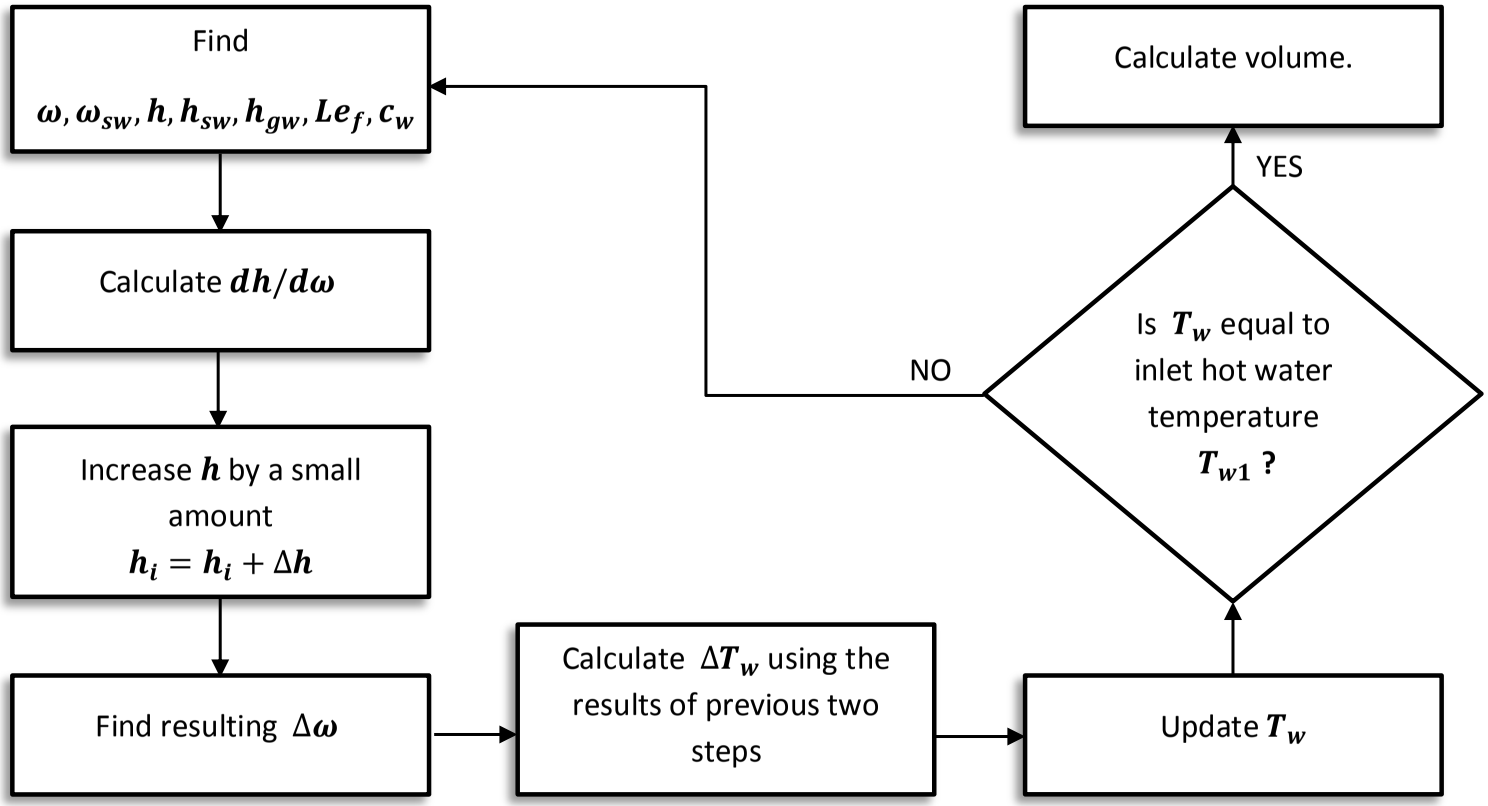

Figure 8: The procedure of tower sizing

According to Brill, selection of 5% ambient wet bulb temperature is common for cooling towers [29]. That is; the hottest five temperatures recorded out of a hundred measurements during recent summer seasons. As reported in ASHRAE handbook, n% annual design condition can be considered as 5n% design condition for the hottest month [30]. Therefore, 1.0% design condition is considered as a reference. The assumptions for sizing can be summarized as the following;

- Sea level barometric pressure
- Uniform cross-section through the tower
- No stray heat transfer with surroundings
- No plume recirculation
- No crosswind effects

Along with the above assumptions, there are two parameters to be decided at the sizing stage: range and approach. *Range* is defined as the difference between hot water inlet temperature and cold water outlet temperature. *Approach* is defined as the difference between cold water outlet temperature and ambient wet bulb temperature. These are illustrated in Figure 9.

In some studies (e.g. [29]), *approach* is referred to the difference with inlet wet bulb temperature instead of ambient wet bulb temperature. It is due to the fact that hot plume *recirculation* and/or *interference* can increase temperature at the tower air inlet. Because recirculation is neglected and because interference occurs when there is more than one tower, the term *approach* refers to both definitions in the upcoming arguments.

As quoted in Zubair and Khan [31], a cooling *approach* to the ambient wet bulb temperature between 3-6 °C is suggested for cooling towers. On the other hand, according to Brill [29], *approach* between 2.8 and 5 °C usually is not economically feasible for power plant use. According to Raju [32], 5.5°C is recommended. Therefore, *approach* has been fixed to 5.5°C; and four degrees of range has been chosen.

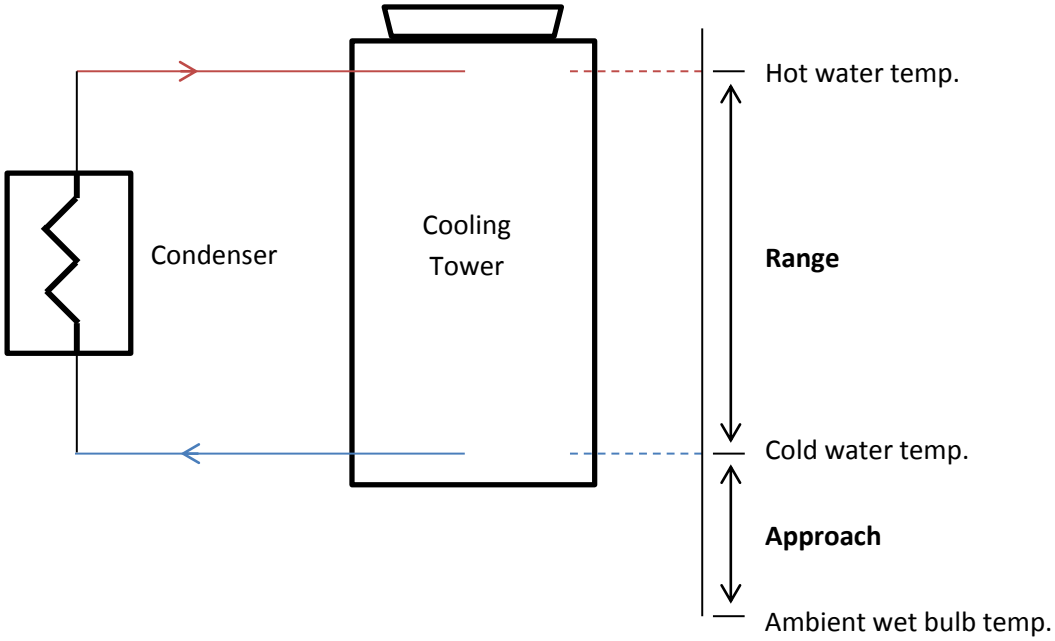

Figure 9: The illustration of range and approach temperatures

Within the present cooling cycle of the system, water flows at a rate of 12.4 kg/s. According to Jones [33], a conventional value for water to air mass flow ratio is unity. Summary of the sizing parameters can be seen in Table 2.

Table 2: Sizing Parameters of the Cooling Tower

PARAMETER	SYMBOL	VALUE
Dry bulb temperature	T	30°C
Wet bulb temperature	T_{wb}	24.4°C
Water temperature at the cooling tower inlet	T_{w1}	33.9 °C
Water temperature at the cooling tower outlet	T_{w2}	29.9°C
Barometric pressure	P_B	101.325 kPa
Mass flow rate of water	$\dot{m}_w$	12.4 kg/s
Mass flow rate of air	$\dot{m}_a$	12.4 kg/s

Using the design parameters given in Table 2, the volume of the fill can be calculated using Equation (12) as defined in [31]:

$$Volume = \frac{\dot{m}_a}{H_d a}\int_{w_1}^{w_2} \frac{d\omega}{\omega_{sw} - \omega} \tag{12}$$

Using a dummy function $F(w) = (w_{sw} - w)^{-1}$ as seen in Figure (9), the volume can be found the area under the curve, after being corrected by a constant characterized by fill type.

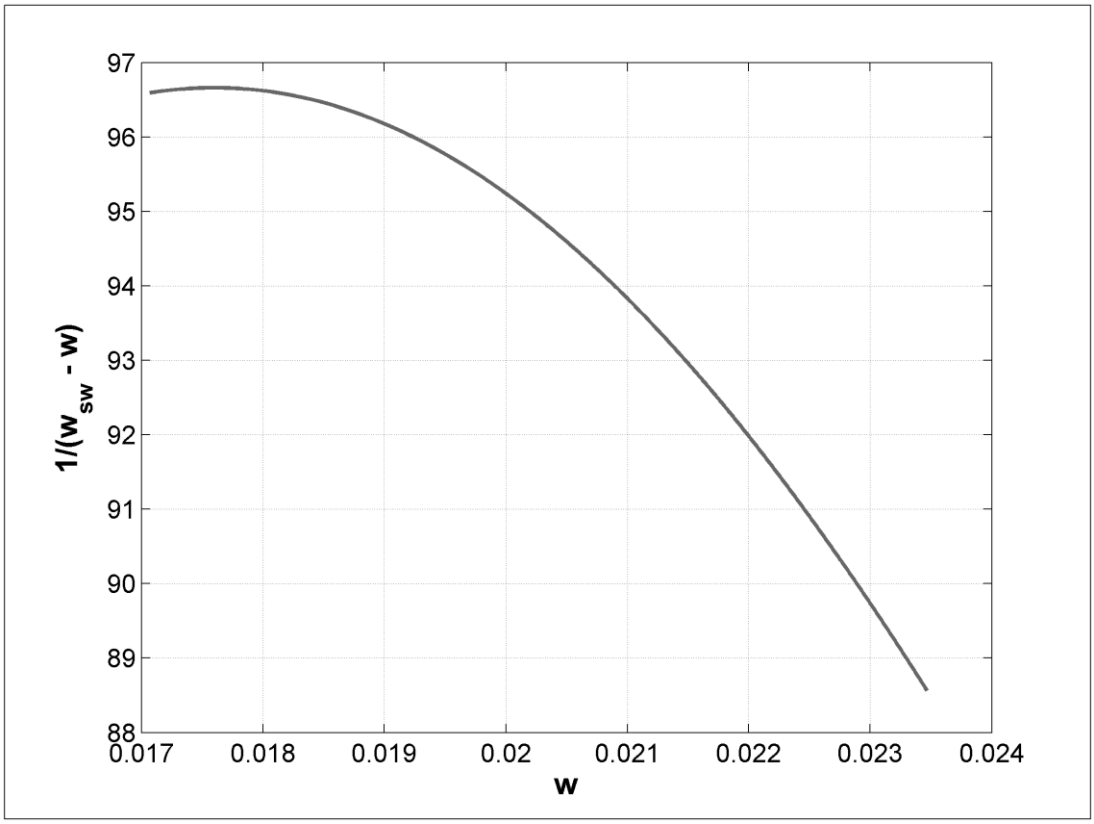

Figure 10: Function F(w)

For the design, flat asbestos sheets are considered as the packing type, for which the term, $H_d a A_{fr}/\dot{m}_w$, appears as 0.459 m^{-1} [9]. Finally, volume of the cooling tower heat transfer surface is found as: 4.25 m^3. Design summary can be seen in Table 3.

Table 3: Design summary of cooling tower

PARAMETER	VALUE
Packing type	Flat asbestos sheets
Rain density*	13,778 kg h^{-1} m^{-2}
Fill width	1.8 m
Fill depth	1.8 m
Fill height	1.31 m
Tower width	2.1 m
Tower depth	2.1 m

* Values over 15,000 kg $h^{-1}m^{-2}$ are not acceptable as reported in [34].

Fan power driving air is obtained via Equation (13) in which pressure drop includes losses for the fill and drift eliminator.

$$\dot{W}_{fan} = \frac{1}{\eta_{fan}} \frac{\dot{m}_a}{\rho_a} \Delta P_{loss} \tag{13}$$

A similar procedure is used for characterizing cooling tower's off-design performance. Starting with an initial guess, exit water temperature can be obtained by an iterative procedure which compares inlet temperatures after sweeping the whole fill volume. On convergence, one can calculate the total heat transfer using the following equation:

$$\dot{Q} = \dot{m}_w c_{p,w} (T_{w1} - T_{w2}) \tag{14}$$

Water Consumption

It is possible to calculate the make-up water requirements determined by the sum of evaporation, blowdown and drift losses. Evaporation loss can be calculated using the difference in the humidity ratios at the cooling tower's inlet and exit as shown in the following expression:

$$E = \dot{m}_a (\omega_2 - \omega_1) \tag{15}$$

Blowdown loss depends on the concentration of dissolved matters in circulating water, which can be quantified through *cycles of concentration,*

(π_c). Mohiuddin and Kant [34] states that cycles of concentration is generally in the range of 3 to 7. Here, it is considered as 5 to to represent blowdown and drift losses as given in Equation (16) as suggested by [35].

$$B + D = E/(\pi_c - 1) \quad (16)$$

Make-up water requirement is found by summing up three elements of water consumption. For the design condition, expected make-up water requirement is calculated as 358 kg/hour owing 286 kg/hour to evaporative losses. This amount corresponds to 0.8% of the inlet water mass flow rate.

CHAPTER 3

ANALYSIS OF DRY COOLING

This chapter elaborates the procedure of selection and sizing of a dry cooling unit for the same ambient conditions used in cooling tower design. Although there are numerous considerations in cooling unit design such as thermal effectiveness, durability, reliability, capital cost etc., the optimal design is beyond the scope of this study and the dry cooling unit is selected using off-the shelf components to accommodate the same cooling load as the wet cooling unit at the same design conditions.

Parallel to the approach taken in the analysis of wet cooling tower is adopted for the analysis of air cooled heat exchanger and handled in two successive stages; namely, sizing/selection and simulation. This chapter mainly based on the former, while the results of simulations are discussed in following chapters. At the end of chapter, a more effective dry cooling unit is considered which can provide insights on the possible improvements on performance limits for the air-cooled heat exchangers.

Surface selection

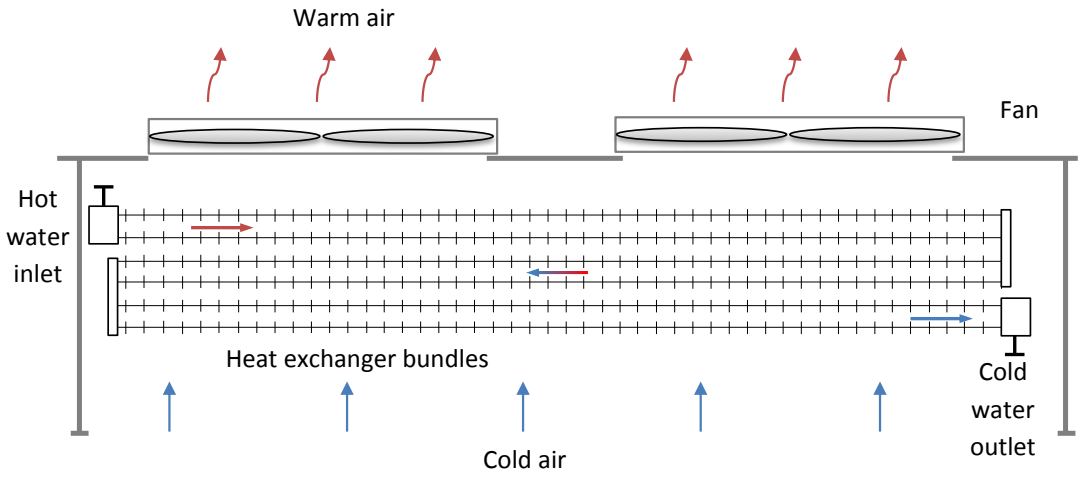

Figure 11: Multi-pass Crossflow Air Cooled Heat Exchanger

The dry cooling unit considered for assessment is a multi-pass cross-flow air-cooled heat exchanger (shown in Figure 11), in which closed loop water removes heat from the refrigerant and rejects it to the ambient air mainly by convection. For the surface of the heat exchanger, a staggered individually finned circular tube configuration is selected for the base design (CF-9.05-3/4J (B) in Kays and London [36]), as shown in Figure 12.

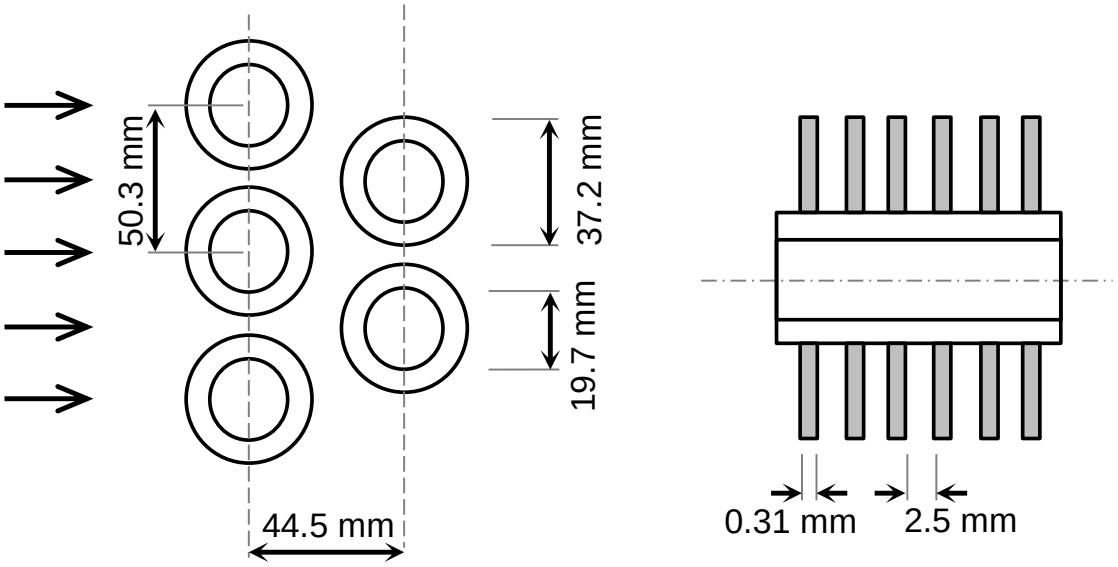

Figure 12: Staggered individually finned tube surface: CF-9.05-3/4J (B)

This surface is considered because it is off-the-shelf and the heat transfer and pressure drop correlations are already provided. Staggered configuration (Figure 13(b)) is preferred over its inline configuration counterparts (Figure 13(a)) because it generally achieves better heat transfer rates for higher number of rows especially for low Reynolds number [37]. The idea behind usage of fins is to compensate for poor heat transfer characteristic on the air aide by increasing the outside surface area.

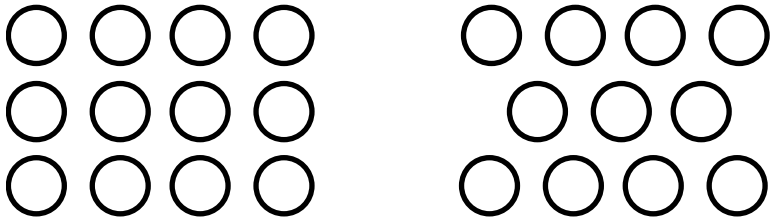

Figure 13: Inline (a) and staggered (b) tube arrangements

One can find the surface characteristics of the surface in Table 4. Tube thickness has been fixed at 4 mm. Materials of the tubes and fins are selected as aluminum and copper, respectively.

Table 4: Surface Specifications

PARAMETER	SYMBOL	VALUE
Inside diameter	d_i	15.66x10^{-3} m
Outside diameter	d_o	19.66x10^{-3} m
Fin tip diameter	d_e	37.2x10^{-3} m
Fin thickness	δ	0.31x10^{-3} m
Fin pitch	P_f	2.89x10^{-3} m
Longitudinal pitch	P_l	44.5x10^{-3} m
Transversal pitch	P_t	50.3x10^{-3} m
Free flow area / Frontal area (air side)	σ_a	0.572 m^2/m^2
Heat transfer area/Total volume	α	279 m^2/m^3

Methodology

Heat exchanger design can be categorized into two groups: Sizing and rating problem. Sizing is the procedure of finding the required heat transfer area for a given heat transfer surface and inlet-exit conditions of heat transfer fluids. Rating is the procedure of performance evaluation for a heat exchanger surface of predefined size. The two well-known methods, i.e. Logarithmic Mean Temperature Difference method (LMTD) and

effectiveness-NTU, can be used to design a heat exchanger. Each has its own limitations. Effectiveness-NTU method is more suitable to find outlet temperatures and heat transfer rates once the inlet conditions are known. Both methods lead to very same results [38], but effectiveness–NTU is often preferred for compact heat exchanger design [39]. Effectiveness–NTU will be used for both sizing and rating of the air cooled heat exchanger throughout the design process.

Thermophysical properties, i.e. density, dynamic viscosity, specific heat and thermal conductivity of air and water are obtained by the correlations provided in Appendix A, in which they are represented as a function of temperature. They are all evaluated at the arithmetic mean temperature (in Kelvin).

Heat capacity rates for air and water are defined based on the respective mass flow rates, $\dot{m}$, and specific heat capacities, c_p, as given in the following equation:

$$C_a = \dot{m}_a \, c_{p,a} \;\; , \;\; C_w = \dot{m}_w \, c_{p,w} \tag{17}$$

Water mass flow rate is considered as 12.4 kg/s while mass flow rate for air stream depends on the fan speed, and can be represented by the inlet air velocity, u_∞, density, ρ_{a1}, and the frontal area of the heat exchanger, A_{fr} using the following equation:

$$\dot{m}_a = \rho_{a1} \, u_\infty \, A_{fr} \tag{18}$$

The parameters relevant to the effectiveness-NTU method are given in the following equation:

$$C_{min} = \min(C_a, C_w) \,, \;\; C_{max} = \max(C_a, C_w), \;\; C^* = \frac{C_{min}}{C_{max}} \tag{19}$$

The actual heat transfer rate can be calculated based on the theoretical maximum heat transfer rate as shown in the following equation:

$$\dot{Q} = \varepsilon C_{min} (T_{w1} - T_{a1}) \tag{20}$$

where subscripts a and w represent air and water, respectively. Inlet and exit temperatures are illustrated in Figure 14.

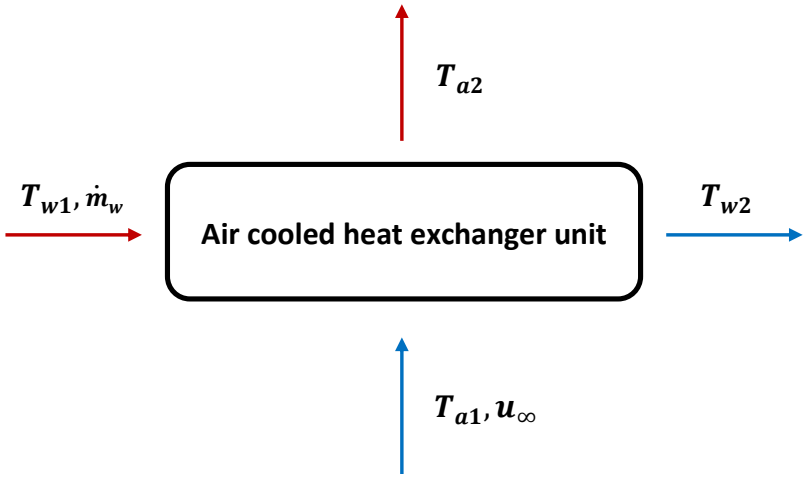

Figure 14: Simplified illustration of inlet and outlet conditions

Heat exchanger effectiveness, ε, in cross flow arrangement can be calculated using Equation (21) for a single pass depending on where C_{max} occurs [37].

$$\varepsilon_p = \frac{1 - exp(-C^*(1 - \exp(-N)))}{C^*} \quad \text{for } C_{max} = C_a$$
$$\varepsilon_p = 1 - exp\left(-\frac{1 - exp(-NC^*)}{C^*}\right) \quad \text{for } C_{max} = C_w \tag{21}$$

These relations hold within each pass. The following relation is suggested for overall counterflow multi-pass crossflow arrangement where fluids are mixed between passes [40]. The illustration of this arrangement can be seen in Figure 15.

$$\varepsilon = \frac{\left(\frac{1 - \varepsilon_p C^*}{1 - \varepsilon_p}\right)^{n_p} - 1}{\left(\frac{1 - \varepsilon_p C^*}{1 - \varepsilon_p}\right)^{n_p} - C^*} \tag{22}$$

where n_p represents number of passes, and C^* stands for heat capacity rate ratio. N is the number of transfer units (NTU) as given in the following equation:

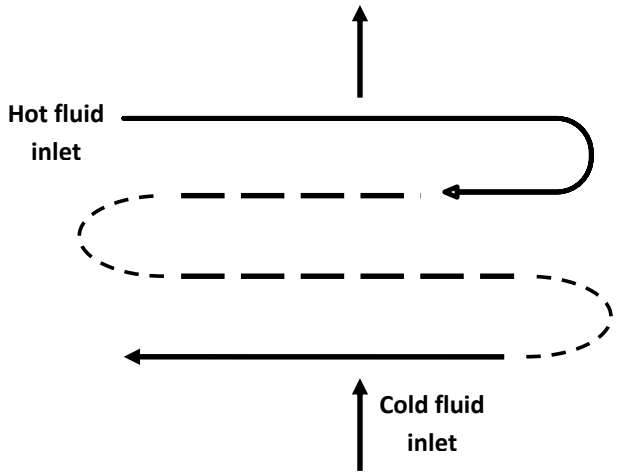

Figure 15: Overall Counterflow, Multi-pass Crossflow arrangement

$$N = UA/C_{min} \tag{23}$$

In Equation (23), overall heat transfer coefficient, UA, can be computed using Equation (24) for a region between two fins and Equation (25) to represent the whole volume.

$$UA^* = \left(\frac{1}{H_w\,\pi\,d_i\,P_f} + \frac{ln(d_o/d_i)}{2\pi\,k_{Cu}\,P_f} + \frac{1}{H_a(\eta_f\,A_f\,+\,A_r)}\right)^{-1} \tag{24}$$

$$UA\;=\;UA^* n_t\,L/P_f \tag{25}$$

where H represents the convective heat transfer coefficient, k_{cu} is the thermal conductivity of the pipe, η_f, is the fin efficiency, n_t is the number of tubes, L is effective length of the tubes, and P_f is the fin pitch. The overall heat transfer coefficient (U) is considered with the inner surface area.

Computations of heat transfer coefficients consider the flow conditions of air and water. The air side convective heat transfer coefficient is found through the following equation:

$$H_a = j\left(\frac{\rho_a u_{max} c_{p,a}}{{Pr_a}^{2/3}}\right) \tag{26}$$

where u_{max} is the maximum velocity across the tubes (which is the free stream velocity divided by the porosity) and j is the Colburn modulus.

Colburn modulus can be represented as a function of Reynolds number for a particular surface configuration. The figure based data in Kays and London [36] is converted into the form shown in Equation (27) for the surface in consideration via regression analysis.

$$j_{base} = 0.01015\left(\frac{Re_a}{1000}\right)^{-0.32263} \tag{27}$$

where Re_a represents the Reynolds number for air flow and represented in the following equation:

$$Re_a = \frac{\rho_a u_{max} d_{ha}}{\mu_a} \tag{28}$$

Air side hydraulic diameter,d_{ha}, is based on the ratio of porosity and surface compactness ($4\sigma/\alpha$). Water side convective heat transfer coefficient is calculated using the following equation:

$$H_w = \frac{k}{d_i} 0.0265\, Re_w^{0.8} * Pr_w^{0.3} \tag{29}$$

Water side hydraulic diameter, d_i, and Reynolds number, Re_w, are computed using Equation (30). Calculation details of air and water properties are provided in the appendix.

$$Re_w = \frac{\dot{m}_w d_i}{n_t A_i \mu_w} \tag{30}$$

Non-circular tubes in the absence of sharp corners, heat and mass transfer correlations for circular pipes can also be applied to non-circular ducts by substituting hydraulic diameter for diameter [41] to be used along with Equation (31).

$$A_i = \pi\, {d_i}^2/4 \tag{31}$$

Sizing Considerations

A conservative cooling unit design must be performed to be able to compensate for the temperature increase and the resulting decrease in cycle efficiency due to the increase in turbine backpressure during the summer

seasons. However, peak temperature periods should be omitted in order to mitigate excessive costs associated with an overdesign. According to Zubair and Khan [31], 10°C approach to dry bulb temperature can be taken as a limit for an economical air cooled heat exchanger design. Thus, design outlet cold water temperature is fixed at 40°C. Table 5 summarizes the design requirements.

Table 5: Summary of the design requirements

PARAMETER	SYMBOL	VALUE
Dry bulb temperature	T	30°C
Water temperature at the heat exchanger inlet	T_{w1}	44°C
Water temperature at the heat exchanger exit	T_{w2}	40°C
Barometric pressure	P_B	101.325 kPa
Mass flow rate of water	$\dot{m}_w$	12.4 kg/s

After deciding on design inlet and outlet temperatures, the parameters relevant to sizing need to be identified. These include:

- number of passes, n_p,
- air mass flow rate, $\dot{m}_a$,
- number of tubes, n_t, and
- length of tubes to characterize the total heat transfer area,A.

A trial and error methodology is employed for sizing, which involve tube length, L, number of tubes, n_t, and mass flow rate of air, $\dot{m}_a$. Following constraints are considered.

- Ratio of tube length to bundle width is kept within 3-3.5 to mitigate extra header costs.
- Velocity of water inside tubes is considered to be in the range of 0.9-2.4 m/s [42].
- Water side pressure loss must not exceed 69 kPa.

First, heat exchanger height is set by considering six tube rows to face the cross-flow. Once the height is fixed, a successful combination of n_t and L for a given air flow rate, $\dot{m}_a$, are sought. Trials are carried out by inserting six rows of tubes to the bundle at a time until the required cooling capacity is achieved. Note that whenever a new row is added to the bundle, tube length is also modified to accommodate the constraint defined above.

Trials are also used to address the number of passes, n_p, which enhances heat transfer and helps fouling control inside the tubes while excessive use would cause water side pressure drop to increase.

Final consideration is relevant to the fan speed. It is possible to reduce heat transfer area for increased air mass flow rate. In return, higher mass flow rates necessitate more fan power, which negatively affects the overall system efficiency. In addition, air side pressure drop dictates limits on fan speed. The fan power can be estimated using the following equation:

$$\dot{W}_{fan} = \frac{1}{\eta_{fan}} \frac{\dot{m}_a}{\rho_a} \Delta P_{loss} \tag{32}$$

where ρ_a is the air density and η_{fan} is the fan efficiency. Pressure loss, ΔP_{loss}, is relevant to the surface geometry. Friction factor, f_{base}, used for computing air side pressure drop is adopted from Kays and London [36] by using regression analysis for the graphs illustrating experimental data to yield the following equation:

$$f_{base} = 0.05025 \left(\frac{Re_a}{1000} \right)^{-0.24402} \tag{33}$$

A range of air mass flow rates (ensuring turbulent flow for enhanced mixing) is considered to evaluate the corresponding heat transfer area as shown in Figure 16, which also shows the heat transfer area and corresponding pressure drop considered in the present study.

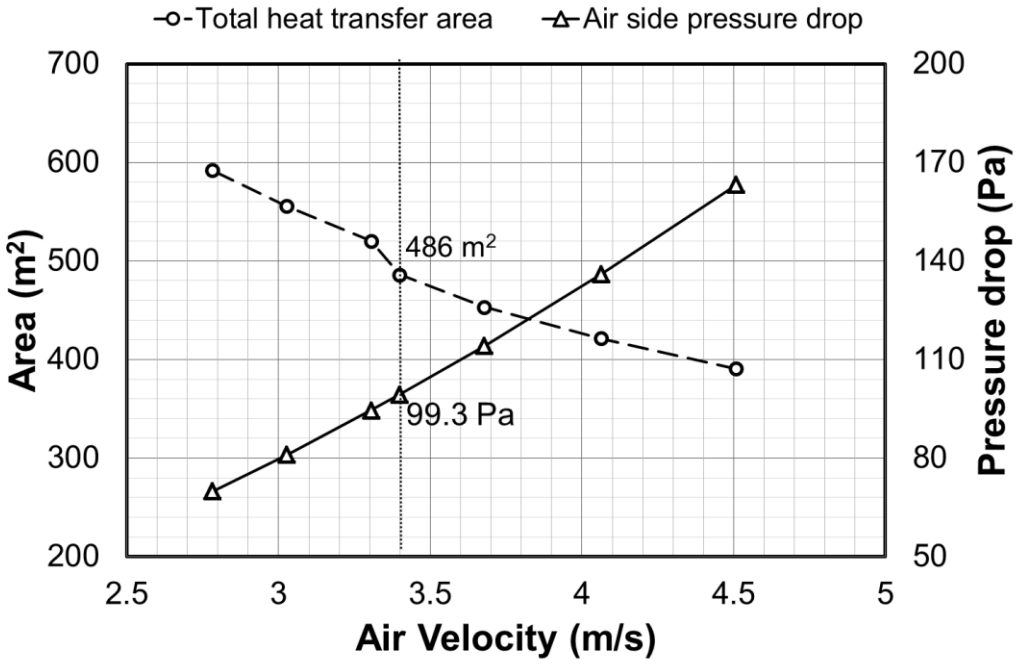

Figure 16: Total heat transfer area vs. air side pressure drop with respect to air velocity

Off-design performance of dry cooling unit is evaluated using ε-NTU method by setting mass flow rates of air and water, inlet temperature of water to calculate the total heat transfer rate at a specified ambient dry bulb temperature via Equation (20). Then, exit temperature of water can be calculated using Equation (34).

$$T_{w2} = T_{w1} - \dot{Q}/C_w \tag{34}$$

Design summary

Table 6 summarizes the characteristics of the selected dry cooling unit, which is to be compared with wet cooling in performance.

Table 6: Air cooled heat exchanger design summary

PARAMETER	SYMBOL	VALUE
Tube Length	L	4.6 m
Number of tubes	n_t	174
Number of passes	n_p	3
Inlet face velocity	u_∞	3.4 m/s
Air side pressure drop	ΔP_a	99.3 Pa
Water side pressure drop	ΔP_w	13,914 Pa

The effectiveness-NTU approach utilized above is summarized in Figure 17. Once the surface geometry, mass flow rates and inlet temperatures are known, it takes an iterative procedure to find respective outlet temperatures. The outlet temperatures are yet unknown but they are needed to find out the average air and water temperatures and hereby calculating the fluid properties. So, the solution procedure starts with a reasonable initial assumption of outlet temperatures. Then the fluid properties are evaluated accordingly. These results yields to number of transfer units and corresponding heat transfer rate and outlet temperatures. If these outlet temperatures do not match to initial assumption of T_{w2} and T_{a2}, then another iteration takes place. The procedure is followed until outlet water and air temperatures match to the initial assumptions.

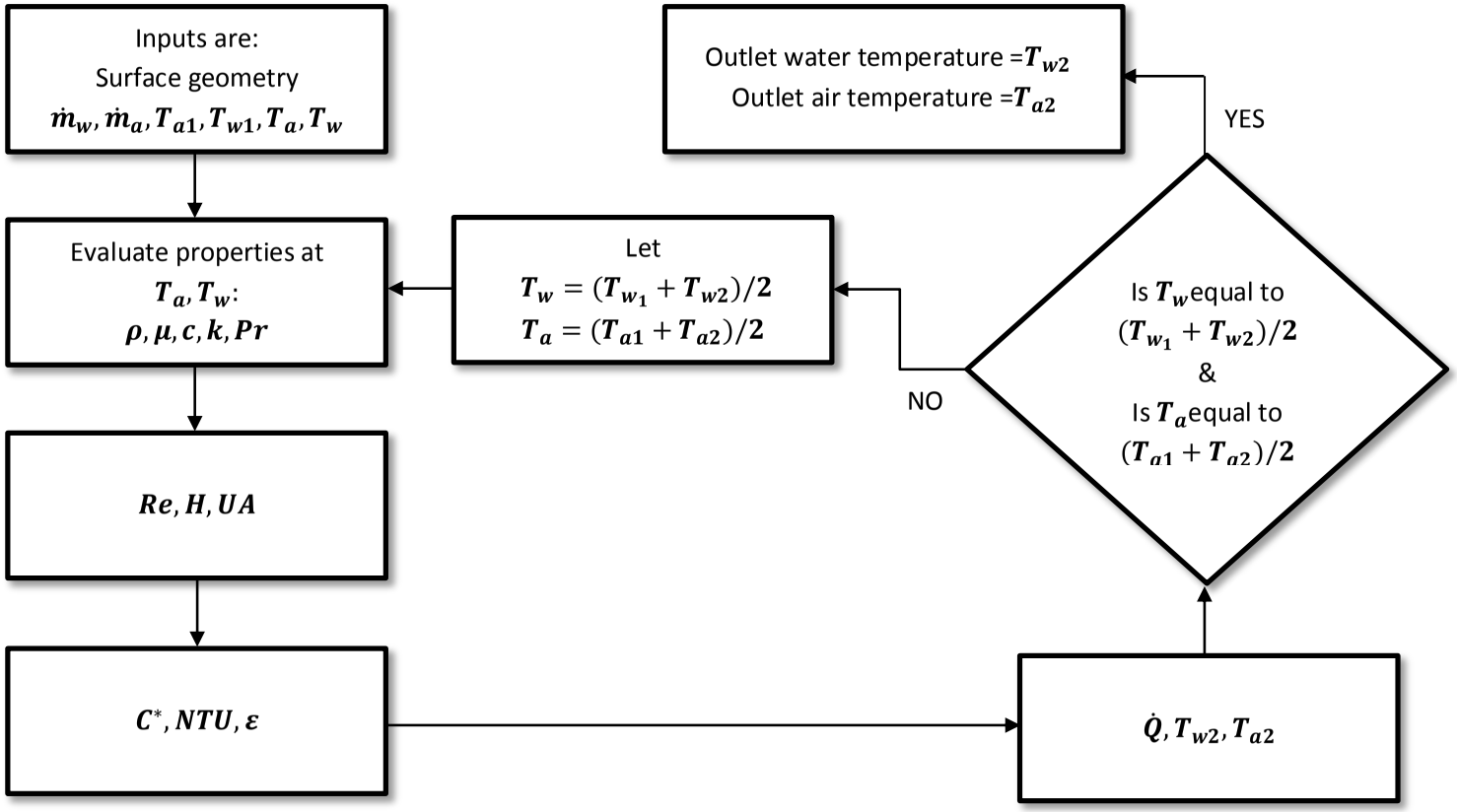

Figure 17: Effectiveness-NTU solution procedure

Re-Design with a more effective heat transfer surface

Plate fin tube surface [11.32-0.737 SR] has the best heat transfer performance characteristics among the options provided in Kays and London [36] and can provide insights on the possible improvements on performance limits for the air-cooled heat exchangers. The surface is illustrated in Figure 18.

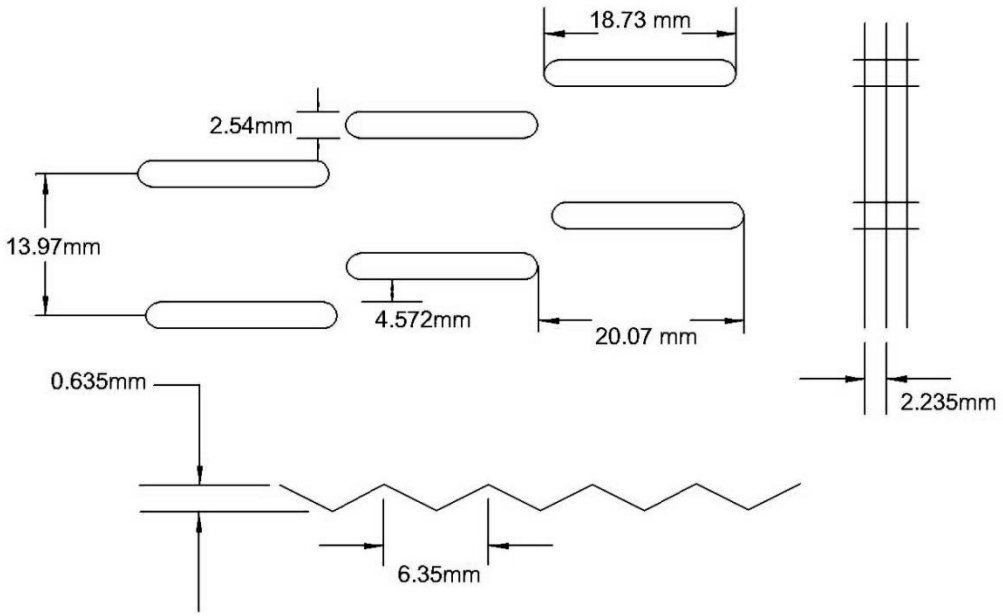

Figure 18: Plate fin tube surface: 11.32-0.737 SR

The enhanced surface considers different geometric parameters yielding a better heat transfer area. One of the differences is that tubes are not circular in contrast to previous case. However, according to Ghiaasiaan, in the absence of sharp corners, heat and mass transfer correlations for circular pipes can also be applied to non-circular ducts by substituting hydraulic diameter for diameter [41]. Another difference is the tube material. Due to the fact that tube walls are fixed at 0.5 mm, steel has been chosen as the tube material. The last difference is the number of passes. Since hydraulic diameter of tubes are much smaller than the previous case,

water side frictional pressure drop becomes more of a concern as number of passes increase.

Also, Colburn modulus, j, in Equation (27), is modified with the following equation:

$$j_{enh} = 0.00998\left(\frac{Re_a}{1000}\right)^{-0.41658} \tag{35}$$

Finally, air-side pressure drop is recalculated using the friction factor correlation for the enhanced surface as given in the following equation:

$$f_{enh} = 0.04237\left(\frac{Re_a}{1000}\right)^{-0.39315} \tag{36}$$

Table 7 shows the design summary. Design summary for both dry cooling units can be found in Appendix C.

Table 7: Design summary of air cooled heat exchanger with an enhanced surface

PARAMETER	SYMBOL	VALUE
Tube Length	L	4.6 m
Number of tubes	n_t	1293
Number of passes	n_p	2
Inlet face velocity	u_∞	3.4 m/s
Air side pressure drop	ΔP_a	134.2 Pa
Water side pressure drop	ΔP_w	36,953 Pa

CHAPTER 4

SYSTEM INTEGRATION

The present chapter integrates the developed dry and wet cooling units' models with an Organic Rankine Cycle (ORC) model to evaluate and compare the overall performance of a CSP system for varying ambient conditions.

Analyses carried out in Chapter 2 and 3 consider conditions only relevant to the cooling units for fixed water inlet temperature. When they operate with an ORC system, the cooling capacity is not only related to the ambient conditions but also to the conditions set by the ORC system. In order to sustain steady state operation, change in the ORC's condenser pressure (and its temperature) can be inevitable. The steady state condition requires that heat rejected from the ORC unit should be the balanced by the heat rejected from the cooling unit. These scenarios can result in different condenser pressures in the ORC system when dry and wet cooling units are individually considered. Hence, a two-way interaction between the ORC system and the cooling unit is required to better evaluate the differences between dry and wet cooling systems.

Wet cooling unit is expected to achieve a lower turbine backpressure and a higher power output due to the difference between dry and wet bulb temperatures. In order to surmount this hurdle, condenser of ORC is resized to match turbine backpressure for both cases. Condenser heat transfer area is taken as 10.99 m^2 for the wet cooling system while it is enlarged to 22.35 m^2 for dry cooling system.

ORC model in consideration is part of a previous study by Bamgbopa [25], which evaluates the performance of an ORC system for a given set of pump, evaporator, twin-screw expander and condenser for a fixed cold temperature reservoir. Present chapter extends Bamgbopa's model [25] to include

changing ambient conditions by considering dry and wet cooling units for fixed design specifications. The integration of ORC and cooling units is illustrated in in Figure 19.

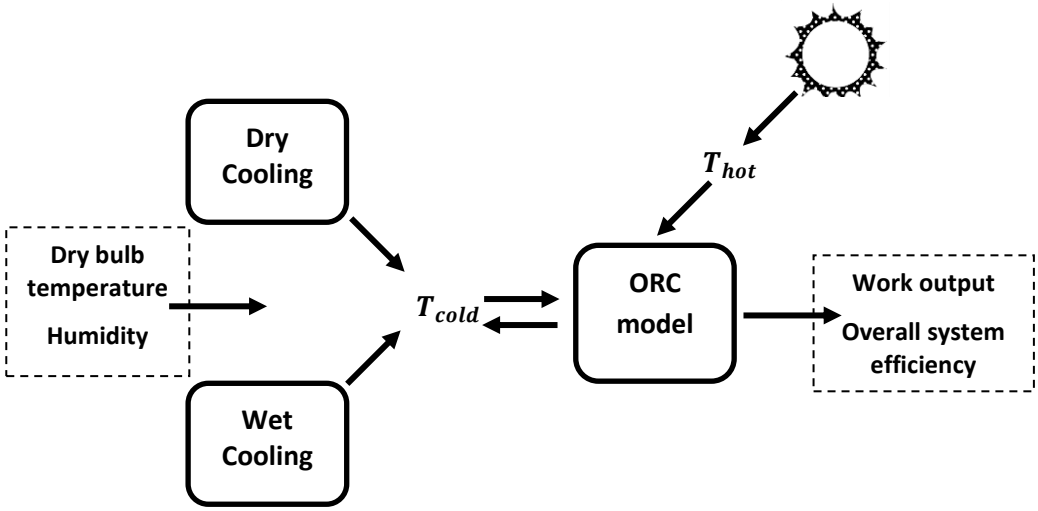

Figure 19: Integration of the two models

Bamgbopa's ORC model [25] considers that heat transfer to the refrigerant (i.e. R245fa) through an evaporator is characterized by the hot fluid's temperature, T_{h1}, and its mass flow rate, $\dot{m}_h$. Pressure ratio of the cycle characterized by the pump for a given refrigerant mass flow rate is utilized to calculate expander's shaft work. Condenser is modeled as a typical counter-flow heat exchanger, which requires cooling fluid's temperature, T_{w2}, and its mass flow rate, $\dot{m}_w$, as inputs. During heat rejection through the condenser, the cooling fluid's temperature, T_{w2}, increases at the exit. Then the cooling fluid (water) at the condenser exit enters either the dry or wet cooling unit to interact with the ambient conditions. The link between the cooling model and the ORC model is established via this cooling fluid's temperature, T_{w2}. Figure 20 illustrates important state temperatures for evaporator and condenser.

Air enters the cooling unit at ambient conditions, i.e. dry bulb temperature of T_{a1}, while water enters the cooling unit at a temperature of T_{w1}. As a

result of the cooling process, air is heated to a temperature of T_{a2} while water is cooled down to a temperature of T_{w2}, which then enters the condenser unit of the ORC. The refrigerant starts condensing from T_1 to the exit state characterized by T_2 while T_{w2} is heated back to recover its original state of T_{w1}.

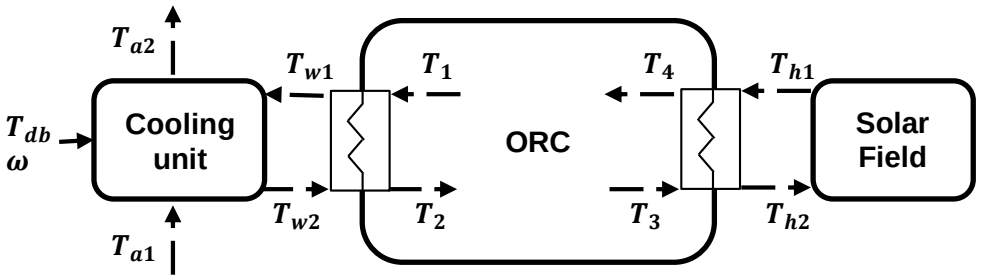

Figure 20: System overview

The blue line in Figure 21 represents the process that water goes through (T_{w2} to T_{w1}) inside the condenser. T_{h1} and T_{h2} represents hot water temperatures circulating between parabolic trough collectors and evaporator. The red line shows the process that water goes through inside the evaporator.

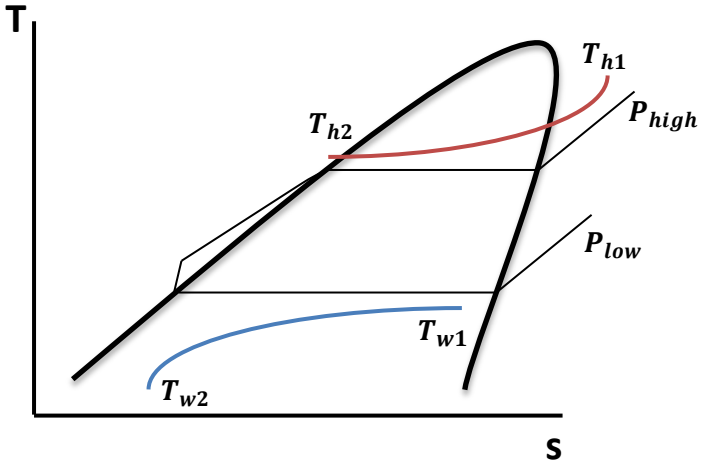

Figure 21: T-s diagram for R245fa and the change of water temperatures through heat exchangers

Integration of ORC and cooling units is summarized in Figure 22. The procedure starts with an initial assumption of inlet water temperature, $T_{w1}{}^{*}$. Dry or wet cooling unit's model is applied for relevant ambient conditions, i.e. dry bulb temperature, T_{a1}, and relative humidity, φ, to obtain outlet cold water temperature, T_{w2} , which is fed to the ORC model as an input. Starting with an initial guess for condensation pressure, P_{low}^{*} , a combination of T_{w1} and P_{low} is sought to satisfy steady state conditions with complete condensation. The final state at the condenser exit is examined whether the refrigerant can reach to a saturated liquid state or not. If the state is a saturated mixture, condensation pressure (P_{low}) is modified and a new set of steady state conditions for the ORC system are obtained using this new condenser pressure until refrigerant ends up at a saturated liquid state. Once the condenser pressure is found to satisfy complete condensation, temperature at the condenser exit is compared with the initial assumption of water inlet temperature, T_{w1}^{*}. The whole process is repeated until the initial assumption of water inlet temperature matches with the outcome obtained using the ORC model. The final conditions represent the steady state operating conditions for the whole system and performance metrics are analyzed.

During the investigations, the same parameters characterizing system components and the same inputs are used for both dry and wet cooling simulations with the exception of the condenser size. List of common parameters are listed in Table 8.

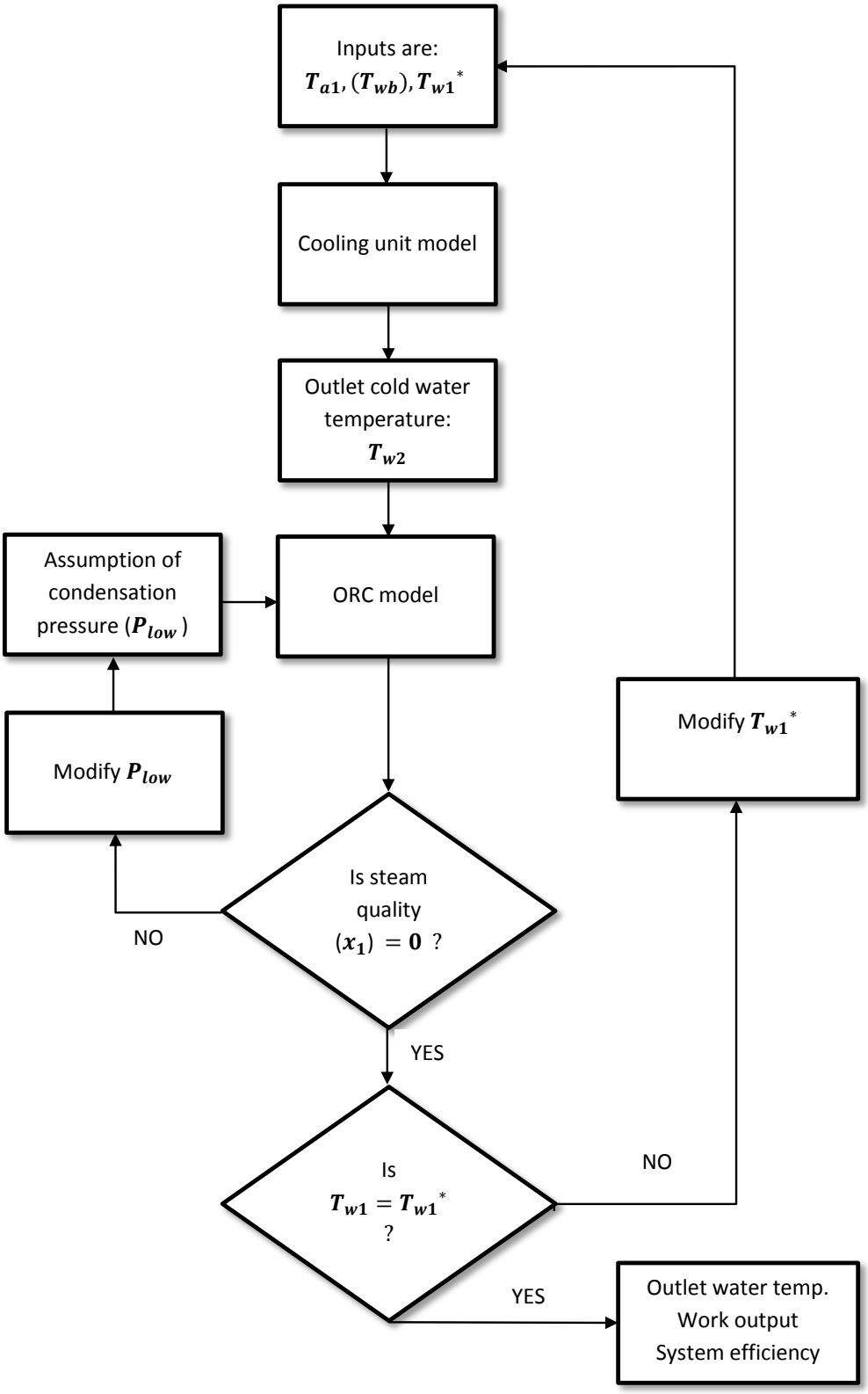

Figure 22: Flow diagram of the system simulation

Table 8: The parameters in common for both configurations

PARAMETER	SYMBOL	VALUE
Hot water mass flow rate	$\dot{m}_h$	12 kg/s
Refrigerant mass flow rate	$\dot{m}_{ref}$	1.5 kg/s
Cold water mas flow rate	$\dot{m}_w$	12.4 kg/s
Barometric pressure	P_B	101.325 kPa
Recirculation		None

Evaporator, on the other hand, is considered to work for hot water temperatures coming from solar field, T_{h1}, varying between 80 °C and 95 °C according to the theoretical solar irradiation at the site. Specifically, months with highest irradiation are considered to bring heat transfer fluid to 95 °C at evaporator's inlet while winter months, when irradiation is lower than the threshold, are not considered as capable of producing power.

CHAPTER 5

RESULTS AND DISCUSSION

In this chapter, the selected wet and dry units, characteristics of which are summarized in Chapter 2 and Chapter 3, are to be compared for their performance. The comparison is established through the following cases:

- Cooling capacity for off-design conditions of isolated units.
- System level energy output of the solar thermal system for off-design conditions.
- System level energy output of the solar thermal system considering daily average and maximum temperatures for a representative year.

Wet cooling unit and dry cooling unit (base surface) are designed for the same cooling load. When ambient conditions, such as dry bulb temperature or relative humidity, deviates from the specified values of Table 1, cooling capacities of each unit is expected to change. This is represented in Figure 24, in which the performances are compared for ±6°C deviation in the dry bulb temperature and ±20 % deviations of relative humidity from the design condition.

Figure 24 shows that increase in dry bulb temperature deteriorates the performance of all cooling units when considered as a standalone unit. Dry unit's response to dry bulb temperature change is very similar to wet cooling tower at design conditions (φ=63%). For humid conditions, (φ=83%), cooling capacity of wet cooling decreases more than dry cooling and for conditions with lower relative humidity (φ=43%) it outperforms dry cooling. Humidity ratio's impact on the cooling capacity increases with the dry bulb temperature.

Figure 25 illustrates the power output of selected units when used with the ORC system. It is seen in Figure 25 that wet cooling unit and dry cooling unit yields the same power output (21.3 kW) at the design conditions

(T=30°C, φ=63%). Base dry cooling unit's cooling capacity deteriorates for higher ambient temperatures while it performs better for lower temperatures. For humid conditions (φ=83%), use of base dry cooling unit yields higher power output while this is reversed when humidity is low. These conditions produce a difference up to 4 kW, which is significant for an ORC producing 25 kW of power. For low ambient dry bulb temperature and high humidity and for high ambient dry bulb temperature and low humidity, dry and wet cooling systems can produce the same work output.

The reason behind decreasing ORC work output for increasing ambient temperatures in Figure 25 can be seen in Figure 23, where refrigerant saturation pressure (condenser pressure) increases continuously from 24°C to 36°C for both dry and wet cooling. Dry cooling unit saves 358 kg of water per hour at the design conditions and a twenty percent deviation in relative humidity off the design value would change the water consumption by 13 kg/hr.

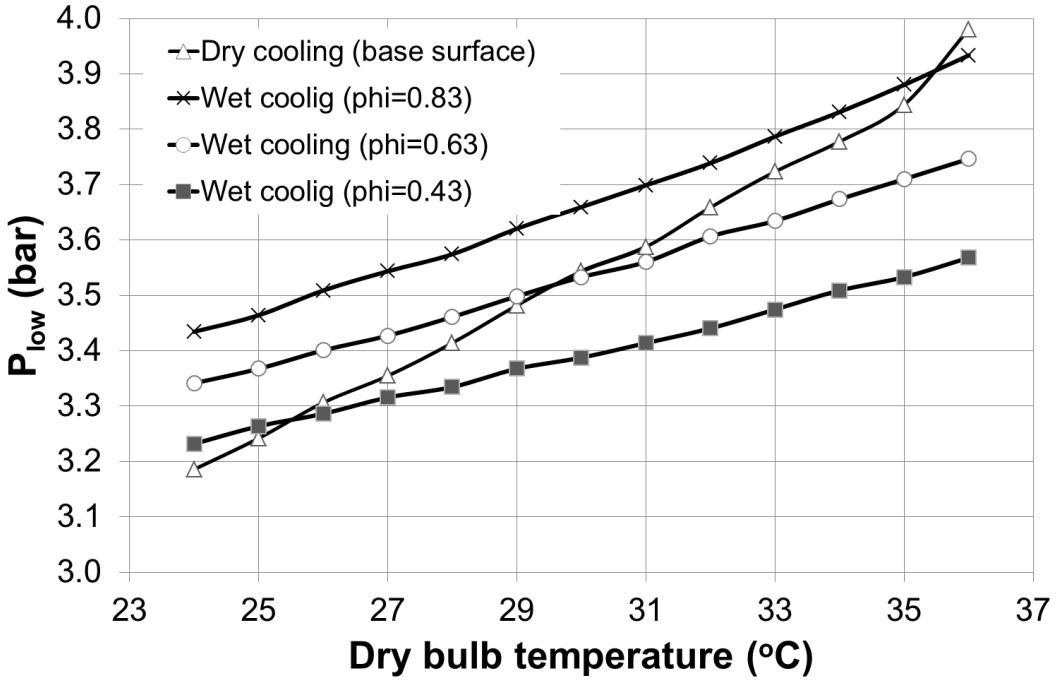

Figure 23: Change of saturation pressure with respect to dry bulb temperature

Feasibility study takes system's location into account to simulate both units for changing ambient conditions and solar irradiation over a year period in Northern Cyprus. Figure 26 shows monthly averages of daily maximum and daily average dry and wet bulb temperatures during a year from September 2011 to August 2012 at the selected site. Figure 26 also shows theoretical global irradiation per day, which characterizes hot water temperature at evaporator inlet. ORC is assumed operational between one hour after the sunrise and one hour before the sunset provided that there is sufficient irradiation for that particular month. Under this condition, the plant stays operational 42% of the whole year.

Net energy production from September 2011 to August 2012 is shown in Figure 27, which accounts for the fan power consumption of the cooling units. Considering daily average temperatures, wet cooling system produces more energy from June to October as dry cooling unit's fan power consumption is higher than the wet cooling unit. The difference between the two is more distinct between July and September especially due to the differences observed in dry and wet bulb temperature in Figure 26. For daily maximum temperatures, energy output with dry cooling system is negatively affected by 500-1500 kWh while wet cooling system shows a slight decrease of 50-150 kWh.

While wet cooling unit is better in energy production, its water consumption is engrossing as shown in in Figure 28 to illustrate possible savings when replaced with a dry cooling unit. Monthly water consumption is shown for each month, except November, December and January when the plant is non-operational. As expected, summer time water consumption is higher than the others due to increased cooling load. Another notable result is that the highest water consumption is realized in July instead of June, although irradiation, heat input and cooling load is lower in the former. The reason is the elevated temperatures in July, which deteriorates cooling performance and increases the evaporation rate per unit of heat rejected.

Table 9 compares the computed water consumption of the power plant in consideration and typical power plants [43] in the basis of water consumed per unit of electricity produced. The big difference in water consumption values between this plant and other utility scale plants emanates from the scale of the power plant. As plant size gets smaller, water evaporation rate per power produced increases.

Table 9: Water consumption for typical plants

Power plant type	Water consumption per unit of electricity produced (ton/MWh)
Solar thermal plant (present study)	16.93
Steam Plant (fossil)	1.9-2.3
Steam Plant (nuclear)	3.0-4.2
Combined-Cycle Plant	0.9

Figure 29 shows net energy production for the enhanced surface dry cooling unit to compare it to the wet cooling units' performance shown in Figure 27 In contrast to previous case, dry cooling case outperformed wet cooling in terms of total work output from February to June. After June, during which the temperatures gets higher and radiation decreases, work output of both systems are still comparable. Although dry cooling with enhanced surface case could have performed better in terms of total energy output, extra fan power negatively affects system efficiency much more than wet cooling. Besides, the difference between dry cooling cases shrinks due to higher fan power requirement of the enhanced surface, for which the air side pressure drop appears to be higher. In the case of dry cooling enhanced surface, however, utilization of a more compact heat exchanger resulted in 0.8-1.1 MWh monthly increase in net electricity output during summer months. Both dry heat exchangers showed lowered performances for elevated temperatures when compared to wet cooling.

Table 10: Electricity production and relative economical performances for all cooling units considered (yearly).

Case	Total electricity production	Net electricity production	Revenue (relative)	Water savings (relative)	Profit (relative)
Wet cooling	50.56 MWh	47.98 MWh	Base	Base	Base
Dry cooling (base)	53.76 MWh	44.98 MWh	- $597	+ $1,310	+ $713
Dry cooling (enhanced)	62.46 MWh	50.75 MWh	+ $551	+ $1,310	+ $1,861

Table 10 reveals relative economical comparison for the three cases using the prices reported in TRNC (electricity price: 0.20 USD/kW-hour; water price: 1.53 USD/ton). Although electricity consumption is higher for dry cooling cases, overall they appear to be more cost effective than wet cooling when savings due to water consumption are included. A simple sensitivity analysis based on water and electricity prices is included in Appendix E.

It is worth to note that capital costs of dry cooling units are generally higher than wet cooling units [8]. In addition, a condenser with higher heat transfer surface will add into the investment cost. However, in some severely water-short areas, these extra costs can be earned back by saving water. Also, humid weather reversely affects the performance of wet cooling. In humid regions, such as coastal towns as this plant is located on, wet cooling partly loses its advantage over dry cooling. Moreover, the fan speed to achieve a certain level of airflow decreases with altitude. Overall, dry cooling systems can be an alternative to wet cooling systems provided that the site is located in low altitude and humid regions.

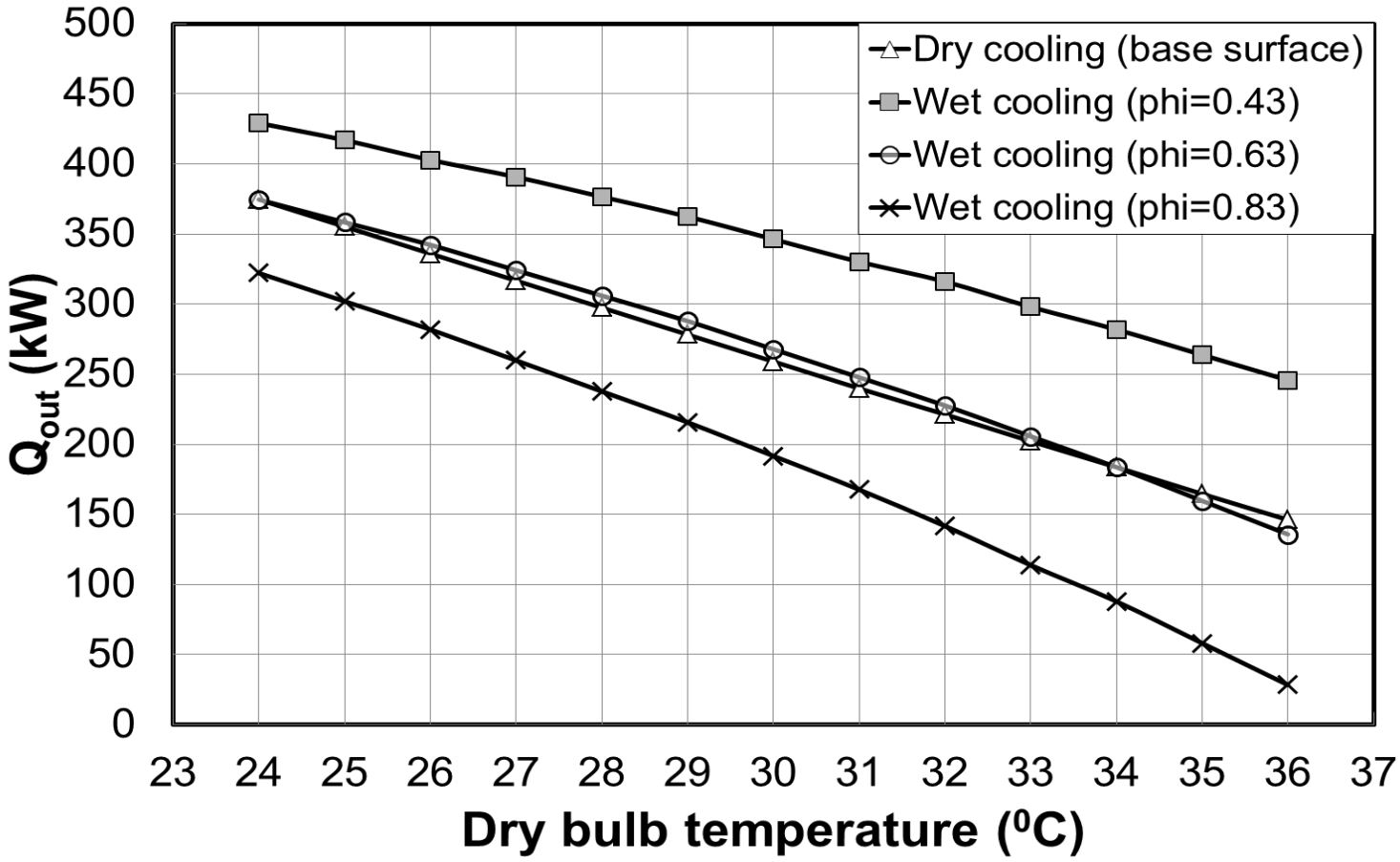

Figure 24: Cooling capacity variation with dry bulb temperature.

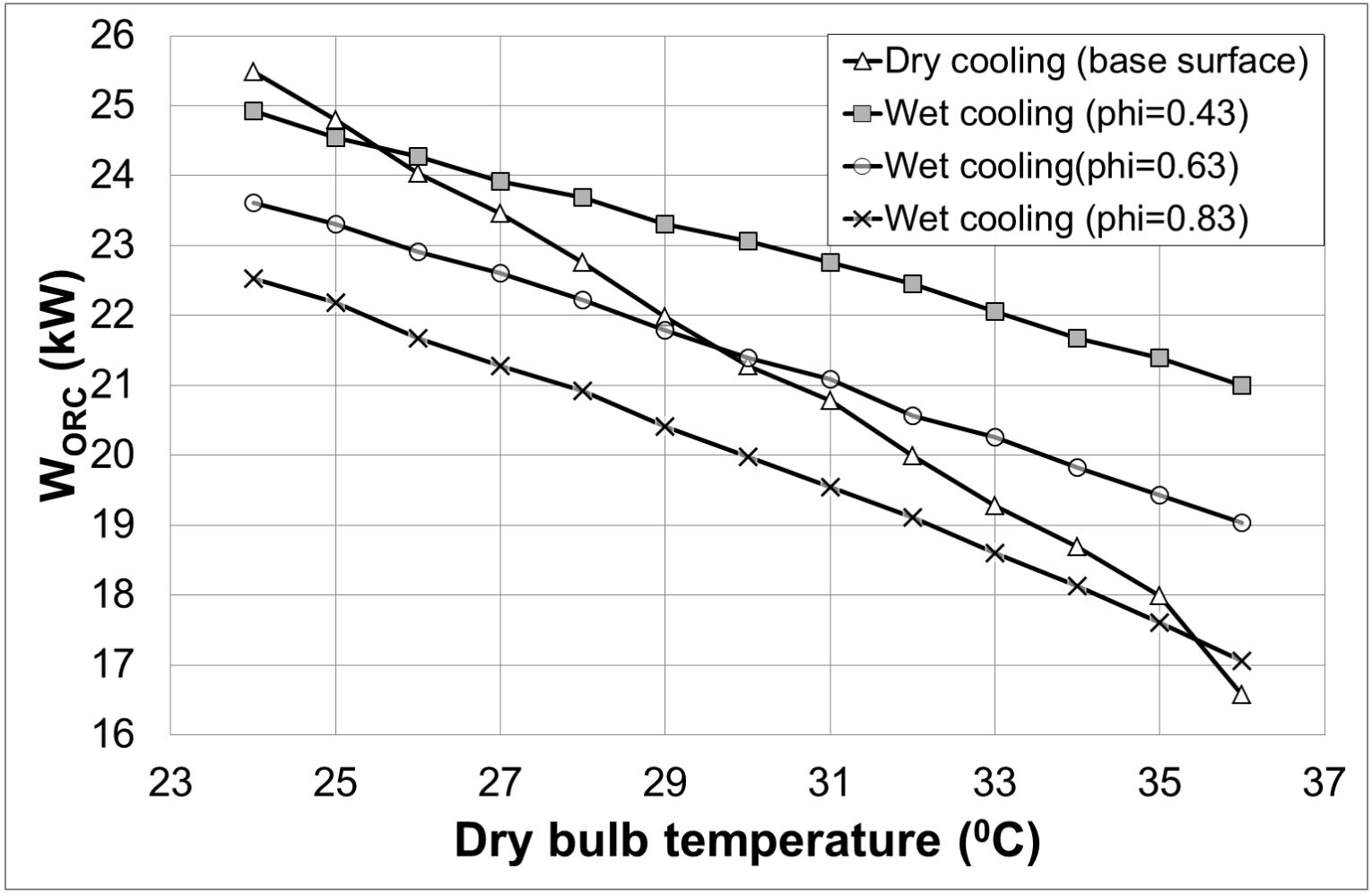

Figure 25: Power output of ORC unit for off-design conditions.

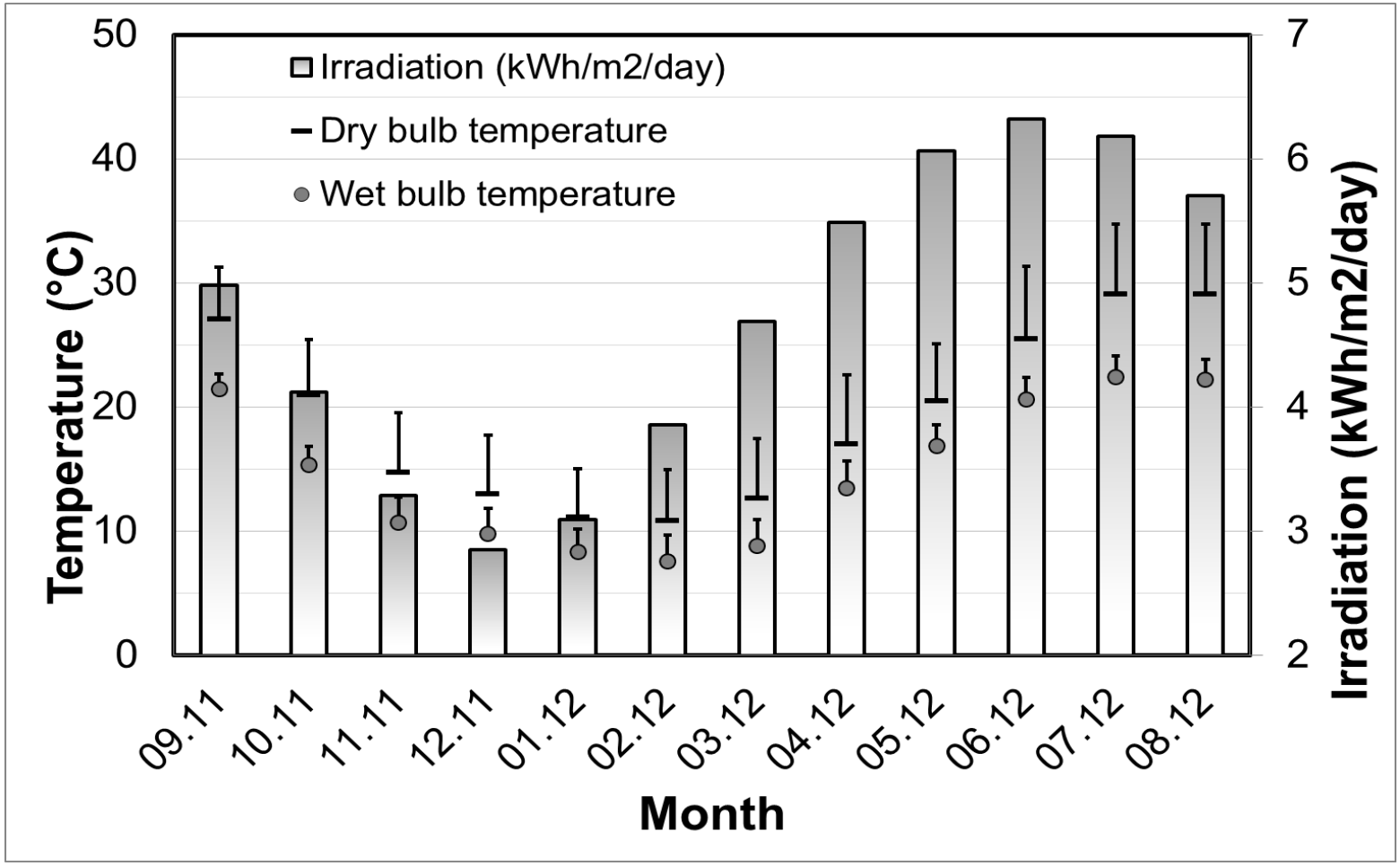

Figure 26: Theoretical irradiation, observed average/maximum dry and wet bulb temperature data at the selected site.

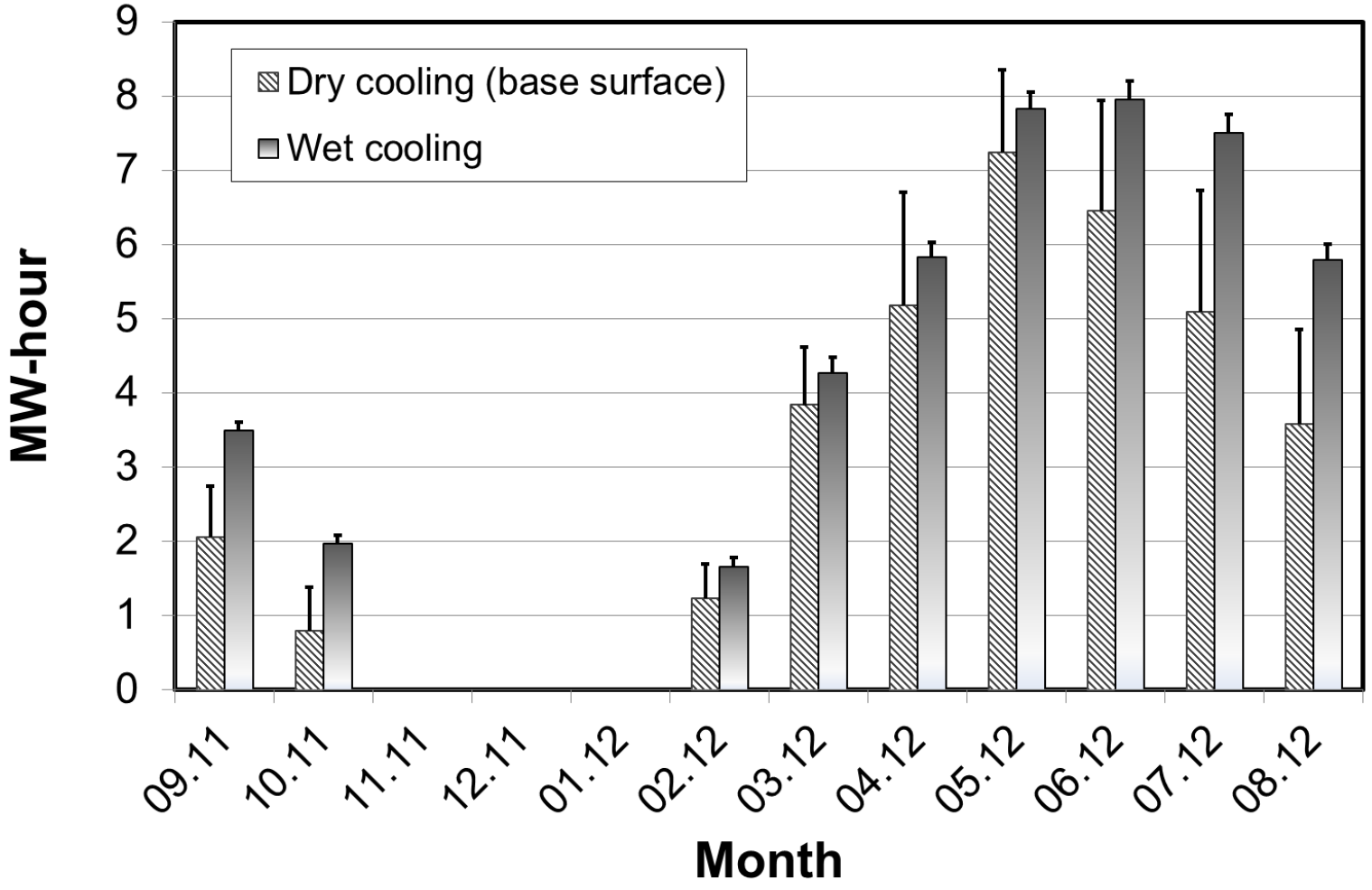

Figure 27: Net electricity produced in MW-hours for dry and wet cooling over one year period.

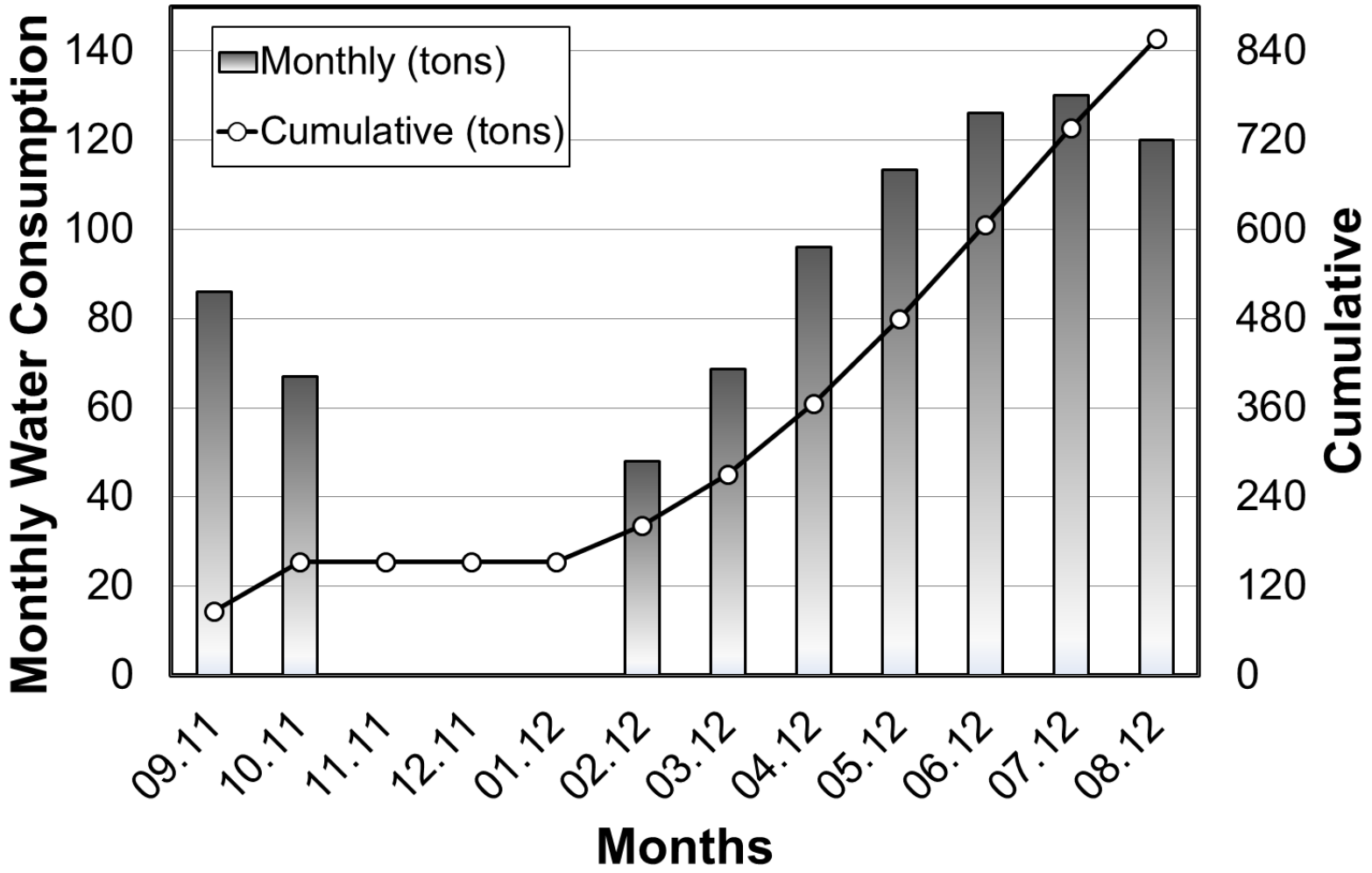

Figure 28: Monthly water consumption during one year period.

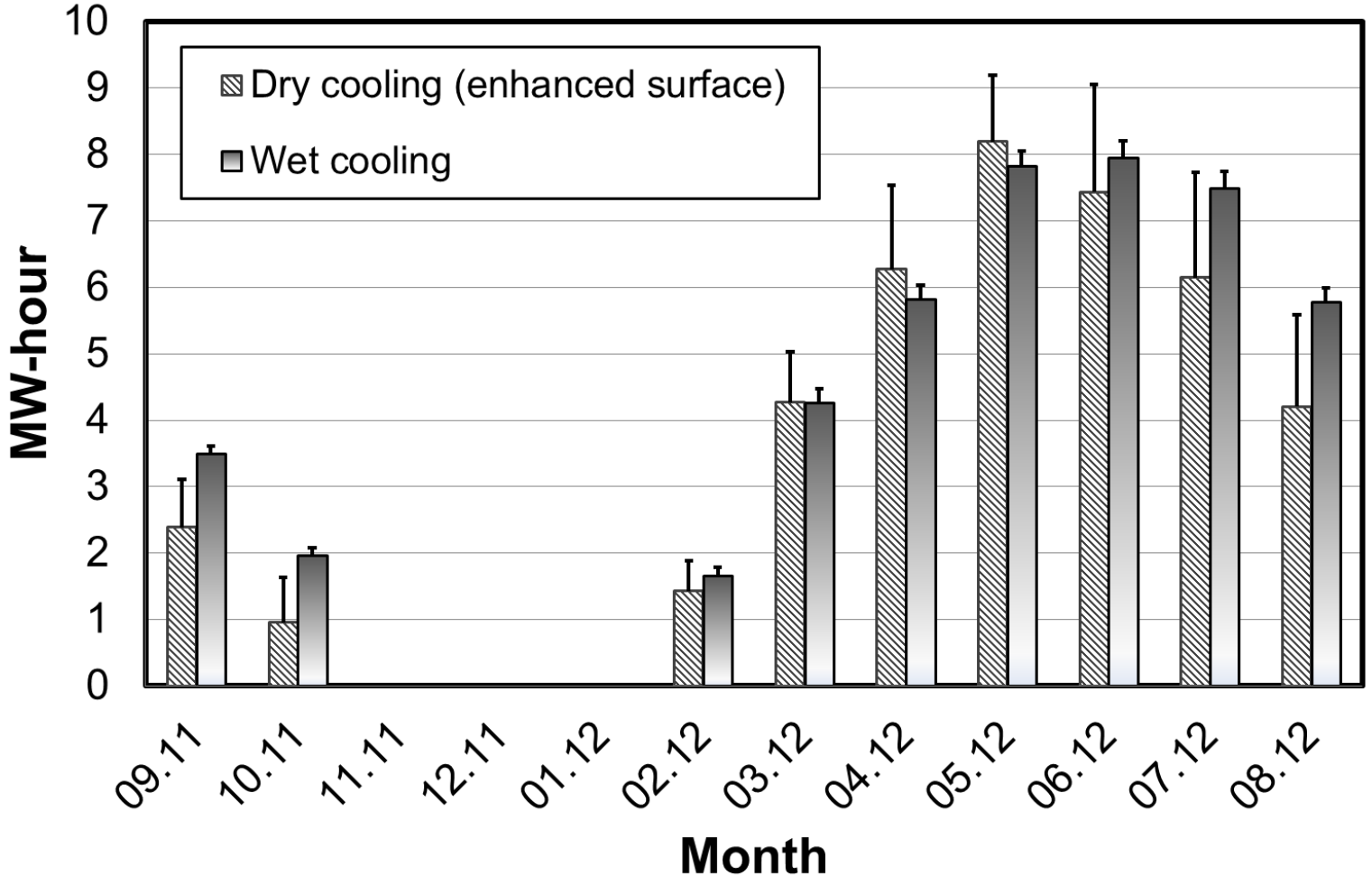

Figure 29: Net electricity produced in MW-hours for dry cooling (enhanced surface) and wet cooling over one year period.

CHAPTER 6

CONCLUSION

The present study illustrates that dry cooling is a notable option to wet cooling for water-short areas in the case of small-scale solar plants. The study location, island of Cyprus, is a good example of humid regions such as remote islands or coastal towns suffering from water scarcity. In such areas, huge saves in water consumption can be achieved by dry cooling with a sacrifice from system efficiency. For this particular case, it corresponded to 3 MWh difference in net electricity production for one year.

As shown, ambient humidity and wet cooling performance are inversely proportional. For a change in 20% in relative humidity, 1.5-2 kW of difference in ORC power output has been observed. As humidity decreases, the performance gap between dry and wet cooling will expand even further. Even though increased condenser area compensates the power deficit, it should be noted that lower efficiency emanated from high fan power requirements. Progress in fan technology and energy-efficient fans are likely to enhance the use of dry cooling. The sensitivity of system throughput to fan power consumption and consideration of state-of-the-art fan technologies can be inspected in more detailed studies. In addition, heat exchanger surfaces with lower pressure drop on the air side will lower fan power requirements, hereby increasing net power output.

As far as present day economic analyses are concerned, dry cooling is labeled as more costly. However, in a world where the prevalence and intensity of water scarcity has been increasing, the validity of these economic analyses can be questioned in two ways. First, these analyses are based on water price, which is a highly site-specific parameter. Second, they are based on today's prices. Nevertheless, as water scarcity gets more widespread, water prices are likely to increase. Therefore, a detailed

economic analysis taking these factors into account and cradle-to-grave lifecycle analyses are to be performed in further studies.

APPENDIX A

Air and Water Property Calculations

Density, dynamic viscosity, specific heat and thermal conductivity are temperature dependent properties. They are all evaluated at arithmetic mean temperature (in Kelvin). Density, ρ (in kg/m^3), viscosity, μ (in Pa s), specific heat, c_p (in kJ/kg K), thermal conductivity, k (W/mK) and the Prandtl number, Pr are obtained through the Equations (37(37)-(44) and coefficients are presented in Table 11 for both air and water.

$$\rho_a = P_a/(R_a T_a) \tag{37}$$

$$\mu_a = a_{11} + a_{12}T_a - a_{13}T_a^2 + a_{14}T_a^3 \tag{38}$$

$$c_a = a_{21} - a_{22}T_a + a_{23}T_a^2 - a_{24}T_a^3 \tag{39}$$

$$k_a = -a_{31} + a_{32}T_a - a_{33}T_a^2 + a_{34}T_a^3 \tag{40}$$

$$\rho_w = (a_{11} - a_{12}T_w + a_{13}T_w^2 - a_{14}T_w^6)^{-1} \tag{41}$$

$$c_w = a_{21} - a_{22}T_w + a_{23}T_w^2 - a_{24}T_w^6 \tag{42}$$

$$\mu_w = 2.414 \times 10^{-5} \times 10^{247.8/(T_w - 140)} \tag{43}$$

$$k_w = -a_{31} + a_{32}T_w - a_{33}T_w^2 + a_{34}T_w^4 \tag{44}$$

Table 11: List of constants used in calculating properties of air and liquid water.

a_{ij}	j=1	j=2	j=3	j=4
Air				
i=1	2.287973×10^{-6}	6.259793×10^{-8}	3.131956×10^{-11}	8.15038×10^{-15}
i=2	1.045356×10^{3}	3.161783×10^{-1}	7.083814×10^{-4}	2.705209×10^{-7}
i=3	4.937787×10^{-4}	1.018087×10^{-4}	4.627937×10^{-8}	1.250603×10^{-11}
Liquid Water				
i=1	1.49343×10^{-3}	3.7164×10^{-6}	7.09782×10^{-9}	1.90321×10^{-20}
i=2	8.15599×10^{3}	2.80627×10	5.11283×10^{-2}	2.17582×10^{-13}
i=3	6.14255×10^{-1}	6.9962×10^{-3}	1.01075×10^{-5}	4.74737×10^{-12}

APPENDIX B

Equations Used in Pressure Drop Calculations

Equations from (45) to (53), which are used for water side pressure drop calculations, are all gathered from the reference [9].

$$\Delta p = \Delta p_i + \Delta p_f - \Delta p_o \tag{45}$$

$$\Delta p_i = (\rho_w \, u_w^2/2\,)\,(1 - \sigma_w^2 + K_c) \tag{46}$$

$$K_c = \left(1 - \frac{1}{\sigma_c}\right)^2 \tag{47}$$

$$\sigma_c = 0.61375 + 0.13318\sigma_w - 0.26095\sigma_w^2 + 0.511146\sigma_w^3 \tag{48}$$

$$\sigma_w = A/(P_t \, P_l) \tag{49}$$

$$\Delta p_f = f_D(L \times pass/d_i)(\rho_w \, u_w^2/2) \tag{50}$$

$$f_D = (1.82 \log_{10} Re_w - 1.64)^{-2} \tag{51}$$

$$\Delta p_o = (\rho_w \, u_w^2/2)\,(K_e - (1 - \sigma_w^2)) \tag{52}$$

$$K_e = (1 - \sigma_w)^2 \tag{53}$$

APPENDIX C

Design Summary for Base and Enhanced Surface Dry Cooling Units

Design outcome			
	Symbol	**Base Surf.**	**Enhanced Surf.**
Tube Length	L	4.6 m	4.6 m
Number of tubes	n_t	174	1293
Number of passes	n_p	3	2
Inlet face velocity	u_∞	3.4 m/s	3.4 m/s
Air side pressure drop	Δp_a	99.4 Pa	134.2 Pa
Water side pressure drop	Δp_w	13,914 Pa	36,953 Pa

APPENDIX D

Temperature and Radiation Data

MONTH	WB (°C)	DB (°C)	Radiation (kW-hour)	Th_1 (°C)
9	21.5	27.04	4.98	86.83
10	15.4	20.96	4.12	81.59
11	10.7	14.73	3.29	0
12	9.76	12.99	2.85	0
1	8.31	11.08	3.09	0
2	7.59	10.82	3.86	80
3	8.79	12.61	4.69	85.06
4	13.5	17.01	5.49	89.94
5	16.9	20.5	6.06	93.41
6	20.6	25.45	6.32	95
7	22.4	29.08	6.18	94.15
8	22.2	29.07	5.7	91.22

APPENDIX E

Basic Sensitivity Analysis Based on Water and Electricity Prices

The area under line represents the combinations of electricity and water prices where dry cooling-base surface is more profitable over wet cooling and vice versa. On the line, two systems are indifferent in terms of revenue.

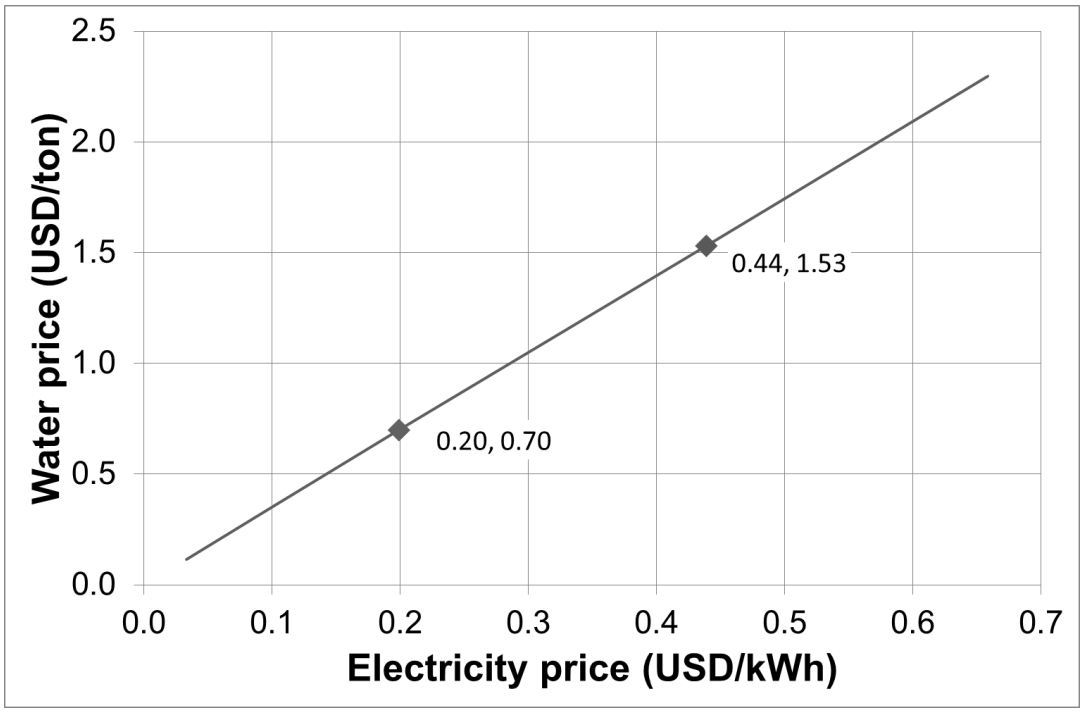

APPENDIX F

Hours of Sunlight

	Hours	Effective Hours	Days	Total Effective Hours
September	12.22	10.22	30	306.6
October	11.10	9.1	31	282.1
November	10.14	8.14	30	244.2
December	9.67	7.67	31	237.77
January	9.91	7.91	31	245.21
February	10.74	8.74	28	244.72
March	11.76	9.76	31	302.56
April	12.89	10.89	30	326.7
May	13.85	11.85	31	367.35
June	14.34	12.34	30	370.2
July	14.13	12.13	31	376.03
August	13.31	11.31	31	350.61
TOTAL	144.06	120.06		3654.05

APPENDIX G

Computer Codes

A function to calculate wet bulb temperature

```
function [Twb] =WetBulb(Tdb, phi)
pabs=101325;
w_s=0.622*(XSteam('psat_T',Tdb)/(1-XSteam('psat_T',Tdb)));
w_correct=0.622/((1+0.622/w_s)/phi-1);
Twb=Tdb-3;
TwbK=Twb+273.16;
z=10.79586*(1-273.16/TwbK) + 5.02808*log(273.16/TwbK)/log(10) +
1.50474*10^-4*(1-10^(-8.29692*(TwbK/273.16-1))) + 4.2873*10^-
4*(10^(4.76955*(1-273.16/TwbK))-1) + 2.786118312;
pvwb=10^z;
w=(2501.6-2.3263*Twb)*(0.62509*pvwb)/(2501.6+1.8577*Tdb-
4.184*Twb)/(pabs-1.005*pvwb) - (1.00416*(Tdb-Twb))/(2501.6+1.8577*Tdb-
4.184*Twb);
while abs(w_correct-w)>0.0001
   if w<w_correct
      Twb=Twb+0.005;
      TwbK=Twb+273.15;
      z=10.79586*(1-273.16/TwbK) + 5.02808*log(273.16/TwbK)/log(10) +
1.50474*10^-4*(1-10^(-8.29692*(TwbK/273.16-1))) + 4.2873*10^-
4*(10^(4.76955*(1-273.16/TwbK))-1) + 2.786118312;
      pvwb=10^z;
      w=(2501.6-2.3263*Twb)*(0.62509*pvwb)/(2501.6+1.8577*Tdb-
4.184*Twb)/(pabs-1.005*pvwb) - (1.00416*(Tdb-Twb))/(2501.6+1.8577*Tdb-
4.184*Twb);
   elseif w>w_correct
      Twb=Twb-0.005;
      TwbK=Twb+273.15;
      z=10.79586*(1-273.16/TwbK) + 5.02808*log(273.16/TwbK)/log(10) +
1.50474*10^-4*(1-10^(-8.29692*(TwbK/273.16-1))) + 4.2873*10^-
4*(10^(4.76955*(1-273.16/TwbK))-1) + 2.786118312;
      pvwb=10^z;
      w=(2501.6-2.3263*Twb)*(0.62509*pvwb)/(2501.6+1.8577*Tdb-
4.184*Twb)/(pabs-1.005*pvwb) - (1.00416*(Tdb-Twb))/(2501.6+1.8577*Tdb-
4.184*Twb);
   end
   end
end
```

Wet cooling function

```
function [Two] = WET(Tw1,Tdb,Twb)
volume=1.3117;
pabs=101325;
inc=0.05;
ma=12.4;
mw=12.4;
hd_a=0.459*mw;
matrix=[];
volume_temp=0;
F=[0];dw=[];
sum=0;
TwbK=Twb+273.15;
z=10.79586*(1-273.16/TwbK) + 5.02808*log(273.16/TwbK)/log(10) +
1.50474*10^-4*(1-10^(-8.29692*(TwbK/273.16-1))) + 4.2873*10^-
4*(10^(4.76955*(1-273.16/TwbK))-1) + 2.786118312;
pvwb=10^z;
Tw=Tw1-10; Two=Tw;
wint=(2501.6-2.3263*Twb)*(0.62509*pvwb)/(2501.6+1.8577*Tdb-
4.184*Twb)/(pabs-1.005*pvwb) - (1.00416*(Tdb-Twb))/(2501.6+1.8577*Tdb-
4.184*Twb);
while abs(Tw-Tw1)>0.1
if Tw<Tw1
   Two=Two+0.03;
else
   Two=Two-0.03;
end
w=(2501.6-2.3263*Twb)*(0.62509*pvwb)/(2501.6+1.8577*Tdb-
4.184*Twb)/(pabs-1.005*pvwb) - (1.00416*(Tdb-Twb))/(2501.6+1.8577*Tdb-
4.184*Twb);
h=(1.006+w*1.805)*Tdb+2501*w;
Tw = Two;
cw=(8.15599*10^3 - 2.80627*10*(Tw+273.15) + 5.11283*10^-
2*(Tw+273.15)^2 - 2.17582*10^-13*(Tw+273.15)^6)/1000;
while abs(volume_temp-volume)>0.0001
   if (volume_temp >= volume) || (volume_temp <0)
      break
   end
w_sw=0.622*(XSteam('psat_T',Tw)/(1-XSteam('psat_T',Tw)));
h_sw=(1.006+1.805*w_sw)*Tw+2501*w_sw;
h_gw=XSteam('hv_T', Tw);
Le=0.866^0.667*((w_sw+0.622)/(w+0.622)-1)/log((w_sw+0.622)/(w+0.622));
ratio=Le*(h_sw-h)/(w_sw-w)+(h_gw-2501*Le);
h=h+inc;
w=w+inc/ratio;
Tw = Tw+ma/(mw*cw)*((inc)-(inc/ratio)*cw*Tw);
```

```
cw=(8.15599*10^3 - 2.80627*10*(Tw+273.15) + 5.11283*10^-
2*(Tw+273.15)^2 - 2.17582*10^-13*(Tw+273.15)^6)/1000;
dw=[dw inc/ratio];
sum=sum+ ((F(end)+1/(w_sw-w))/2*dw(end));
F=[F 1/(w_sw-w)];
volume_temp=ma/hd_a*sum;
end
volume_temp=0;
dw=[];
sum=0;
F=[0];
end
water_loss = (w-wint)*ma*3600*5/4
end
```

Dry cooling function

```
function [Tw2] = DRY(Tw1,Ta1)

%CROSSFLOW DRY COOLING SYSTEM WITH WATER AS THE COOLING
MEDIUM

%---------WATER SIDE----------
%rhow = density (kg/m3)
%kw = Thermal conductivity (W/mK)
%cw = Specific heat (J/kgK)
%muw = Dynamic viscosity (kg/ms)
%Rew = the Reynolds number
%Prw = Prandtl number
%hw = water-side heat transfer coefficient (W/m2K)
%Vw = volumetric flow rate (m3/s)
%mw = mass flow rate (kg/s)
%Cw = heat capacity of water stream
%Tw1 = outlet water temperature (K)
%Tw2 = outlet water temperature (K)
%Tw = bulk water temperature (K)

%---------AIR SIDE----------
%rhoa = density of the air at the bulk temperature(kg/m3)
%rhoa1= density of the incoming air (kg/m3)
%ka = Thermal conductivity (W/mK)
%ca = Specific heat of entering air(J/kgK)
%mua = Dynamic viscosity (kg/ms)
%Rea = airside Reynolds number
%Pra = airside Prandtl number
%ha = air-side heat transfer coefficient (W/m2K)
%ma = air mass flow rate through the face area (kg/s)
```

```
%Ca = heat capacity of airstream
%Ta1 = ambient temperature (K)
%Ta2 = outlet air temperature (K)
%Ta = bulk air temperature (K)
%uinf = velocity of the air (m/s)
%umax = velocity at the min. area
%Ga = mass velocity (kg/m2s)

%---------HEAT EXCHANGER PARAMETERS  -----------
%--------- SURFACE: CF-9.05-3/4J(b)  -----------
%dha = air-passage hydraulic diameter  (m)
%dhw = water-passage hydraulic diameter  (m)
%do = outside diameter (m)
%di = inside diameter (m)
%de = Fin tip diameter (m)
%etaf = fin efficiency
%len = effective length of the tubes (m)
%nt = number of tubes
%delta = fin thickness (m)
%Pf = fin pitch (m)
%Pt = transversal pitch
%A = effective cross-sectional flow area (m2)
%eff = effectiveness of the HX
%kcu = thermal conductivity of copper (w/mK)
%kal = thermal conductivity of aluminum (w/mK)

%N = NTU
%UAi
%UA
%Cmin = min. of Ca and Cw, which is required to find NTU value
%Cmax = max. of Ca and Cw, which is required to find NTU value
%C = Cmin/Cmax
%Qmax = theoretical maximum heat transfer rate from water to the air
%Qact = actual heat transfer rate


%OPERATING CONDITIONS
Tw1=273.15+Tw1;
Ta1=273.15+Ta1;
Tw=Tw1-2;
Ta=Ta1+3;

%HX PARAMETERS
de=37.2*10^-3;
di=15.66*10^-3;
do=19.66*10^-3;
delta=0.31*10^-3;
Pf=2.81*10^-3;
```

```
Pt=50.3*10^-3;
Pl=44.5*10^-3;
sigma=0.572;
alpha=279;
kcu=364;
kal=204;
pass=3;

Vw=45/3600;
uinf=3.4;
nt=174;
len=4.6;
wid=nt/6*Pt;
height=5*Pl+de;
A=pi*di^2/4;
uw=Vw/nt/A*pass;
if uw<0.91 || uw>2.43
   disp('uw beyond limits');
   disp(uw);
end
if (Vw*3600)>54.3
   disp('pump cannot handle this Vw');
end

%-------------   INITIAL STEP   ------------------
%AIR SIDE CALCULATIONS
rhoa1 = 101325/(287.08*Ta1);
mua = 2.287973*10^-6 + 6.259793*10^-8*Ta - 3.131956*10^-11*Ta^2 +
8.15038*10^-15*Ta^3;
ca = 1.045356*10^3 - 3.161783*10^-1*Ta + 7.083814*10^-4*Ta^2 -
2.705209*10^-7*Ta^3;
ka = -4.937787*10^-4 + 1.018087*10^-4*Ta - 4.627937*10^-8*Ta^2 +
1.250603*10^-11*Ta^3;
Pra = mua*ca/ka;

dha = 4*sigma/alpha;
Ga = rhoa1*uinf/sigma;
Rea = Ga*dha/mua;

j=0.01015*(Rea/1000)^-0.32263;
ha=j*Ga*ca/Pra^(2/3);

%WATER SIDE CALCULATIONS
rhow1=(1.49343*10^-3 - 3.7164*10^-6*Tw1 + 7.09782*10^-9*Tw1^2 -
1.90321*10^-20*Tw1^6)^-1;
cw=8.15599*10^3 - 2.80627*10*Tw + 5.11283*10^-2*Tw^2 - 2.17582*10^-
13*Tw^6;
muw=2.414*10^-5*10^(247.8/(Tw-140));
```

```
kw=-6.14255*10^-1 + 6.9962*10^-3*Tw - 1.01075*10^-5*Tw^2 +
4.74737*10^-12*Tw^4;
Prw=muw*cw/kw;
mw=Vw*rhow1;
Rew=mw*di/(nt*A*muw)*pass;
if Rew<=2300
   disp('laminar!');
else
Nuw=0.0265*Rew^0.8*Prw^0.3;
end
hw=Nuw*kw/di;

%FIN EFFICIENCY
b = sqrt(2*ha/(kal*delta));
phi = (de/do-1)*(1+0.35*log(de/do));
etaf = tanh(b*do*phi/2)/(b*do*phi/2);

%OVERALL HEAT TRANSFER COEFFICIENT
UAi=(1/(hw*pi*di*Pf) + log(do/di)/(2*pi*kcu*Pf) + 1/(ha*(etaf*(pi*de^2/4-
pi*do^2/4)*2+pi*do*(Pf-delta))))^-1;
UA=UAi*len*nt/Pf;
ma=rhoa1*uinf*len*wid;
Ca=ma*ca;
Cw=mw*cw;
Cmin=min(Ca,Cw);
Cmax=max(Ca,Cw);
C=Cmin/Cmax;
Qmax=Cmin*(Tw1-Ta1);
N=UA/Cmin;
Np=N/pass;
if Ca>Cw
   eff_p = (1-exp(-C*(1-exp(-Np))))/C ;
else
   eff_p = 1-exp(-(1-exp(-Np*C))/C);
end

eff=(((1-eff_p*C)/(1-eff_p))^pass-1) / (((1-eff_p*C)/(1-eff_p))^pass-C);

Qact=eff*Qmax;
Tw2 = Tw1 - Qact/Cw;
Ta2 = Ta1 + Qact/Ca;

%--------------  ITERATION  ---------------------------
while abs((2*Tw-Tw1) - Tw2)>0.1 || abs((2*Ta-Ta1) - Ta2)>0.1
Tw=(Tw1+Tw2)/2;
Ta=(Ta1+Ta2)/2;

%AIR SIDE CALCULATIONS
```

```
mua = 2.287973*10^-6 + 6.259793*10^-8*Ta - 3.131956*10^-11*Ta^2 +
8.15038*10^-15*Ta^3;
ca = 1.045356*10^3 - 3.161783*10^-1*Ta + 7.083814*10^-4*Ta^2 -
2.705209*10^-7*Ta^3;
ka = -4.937787*10^-4 + 1.018087*10^-4*Ta - 4.627937*10^-8*Ta^2 +
1.250603*10^-11*Ta^3;
Pra = mua*ca/ka;
Rea = Ga*dha/mua;
j=0.01015*(Rea/1000)^-0.32263;
ha=j*Ga*ca/Pra^(2/3);

%WATER SIDE CALCULATIONS
cw=8.15599*10^3 - 2.80627*10*Tw + 5.11283*10^-2*Tw^2 - 2.17582*10^-
13*Tw^6;
muw=2.414*10^-5*10^(247.8/(Tw-140));
kw=-6.14255*10^-1 + 6.9962*10^-3*Tw - 1.01075*10^-5*Tw^2 +
4.74737*10^-12*Tw^4;
Prw=muw*cw/kw;
Rew=mw*di/(nt*A*muw)*pass;
if Rew<=2300
   disp('laminar!');
else
Nuw=0.0265*Rew^0.8*Prw^0.3;
end
hw=Nuw*kw/di;

%FIN EFFICIENCY
b = sqrt(2*ha/(kal*delta));
etaf = tanh(b*do*phi/2)/(b*do*phi/2);

%OVERALL HEAT TRANSFER COEFFICIENT
UAi=(1/(hw*pi*di*Pf) + log(do/di)/(2*pi*kcu*Pf) + 1/(ha*(etaf*(pi*de^2/4-
pi*do^2/4)*2+pi*do*(Pf-delta))))^-1;
UA=UAi*len*nt/Pf;
Ca=ma*ca;
Cw=mw*cw;
Cmin=min(Ca,Cw);
Cmax=max(Ca,Cw);
C=Cmin/Cmax;
Qmax=Cmin*(Tw1-Ta1);
N=UA/Cmin;
Np=N/pass;
if Ca>Cw
   eff_p = (1-exp(-C*(1-exp(-Np))))/C ;
else
   eff_p = 1-exp(-(1-exp(-Np*C))/C);
end
eff=(((1-eff_p*C)/(1-eff_p))^pass-1) / (((1-eff_p*C)/(1-eff_p))^pass-C);
```

```
Qact=eff*Qmax;
Tw2 = Tw1 - Qact/Cw;
Ta2 = Ta1 + Qact/Ca;
end

%Pressure drop calculations
%AIR SIDE
if Rea>7300 || Rea<1800
   disp('Rea beyond the limits of regression!');
end
rhoa = 101325/(287.08*Ta);
rhoa2 = 101325/(287.08*Ta2);
f = 0.05025*(Rea/1000)^-0.24402;
delta_pa =
(rhoa*uinf/sigma)^2/(2*rhoa1)*(f*(alpha*height/sigma)*(rhoa1/rhoa)+(1+sig
ma^2)*(rhoa1/rhoa2-1));
if delta_pa>249 || delta_pa<62
   disp('Air side pressure drop is higher than 124.5Pa!');
end

%WATER SIDE
rhow=(1.49343*10^-3 - 3.7164*10^-6*Tw + 7.09782*10^-9*Tw^2 -
1.90321*10^-20*Tw^6)^-1;
delta_pf = (1.82*log10(Rew)-1.64)^-2*(len*pass/di)*(rhow*(uw)^2/2);
sigma_w = A/(Pt*Pl);
sigma_c=0.61375+0.13318*sigma_w-
0.26095*sigma_w^2+0.511146*sigma_w^3;
K_c=(1-1/sigma_c)^2;
delta_pi = (rhow*uw^2/2)*(1-sigma_w^2+K_c);
K_e=(1-sigma_w)^2;
delta_po=(rhow*uw^2/2)*(K_e-(1-sigma_w^2));

delta_pw =  delta_pi+delta_pf+delta_po;
if delta_pw>6894.7*10
   disp('delta_pw beyond limits');
end
Tw2=Tw2-273.15;
end
```

Steady state ORC simulation

```
clc;clear all;
mhin=12;
%Thin=85;
mcin=12.4;
mref=1.5;
%Acond=10.99;
Acond=22.35;
```

```
A=17.584;

VALUE=0.01;
%Tcout=0;


% MATRIXX=zeros(1,13);
% MATRIX=[24   25  26  27  28  29  30  31  32  33  34  35  36];
% for i=1:1:13
%     MATRIXX(i)=WetBulb(MATRIX(i),0.83);
% end
%MATRIX=[27.04 20.96 14.73 12.99 11.08 10.82 12.61 17.01 20.50 25.45
29.08 29.07];%Akdeniz st 9.11-8.12 avg DB temp
MATRIX=[31.28 25.44 19.57 17.75 15.00 14.96 17.43 22.63 25.10 31.35
34.73 34.73];%Akdeniz st 9.11-8.12 max DB temp
%MATRIXX=[21.47 15.35 10.67 9.76 8.31 7.59 8.79 13.5 16.87 20.62
22.42 22.22];%Akdeniz st 9.11-8.12 avg WB temp
MATRIXX=[22.67 16.83 12.72 11.83 10.17 9.67 10.94 15.67 18.56 22.39
24.11 23.83];%Akdeniz st 9.11-8.12 max WB temp
MATRIX_Thin=[86.83  81.59   0.00    0.00    0.00    80.00   85.06   89.94
93.41   95.00   94.15   91.22];
MATRIX_Tcout=zeros(1,13);
MATRIX_Tcin=zeros(1,13);
MATRIX_wnet=zeros(1,13);
MATRIX_ncycle=zeros(1,13);
MATRIX_qin=zeros(1,13);
MATRIX_plow=zeros(1,13);
MATRIX_phigh=zeros(1,13);
MATRIX_Tlow=zeros(1,13);
Tw1=44;
for eray=[1,2,6,7,8,9,10,11,12]
   Thin=MATRIX_Thin(eray);
   Tcout=Tw1+1;
   while abs(Tcout-Tw1)>0.2
      if Tcout<Tw1
         Tw1=Tw1-0.1
         Tcin=DRYFT(Tw1,MATRIX(eray));
         %Tcin=WET(Tw1,MATRIX(eray),MATRIXX(eray));
      else
         Tw1=Tw1+0.1
        Tcin=DRYFT(Tw1,MATRIX(eray));
        %Tcin=WET(Tw1,MATRIX(eray),MATRIXX(eray));
      end
      Tlow=Tcin+2;
      xexit=1;
      while xexit>VALUE && xexit>=0
         if xexit >0
            Tlow=Tlow+0.1;
```

```
            else
                Tlow=Tlow-0.1;
            end
            if Tlow<=Tcin
                break
            end

--- Bamgbopa's ORC code ---

end
    end
MATRIX_Tcout(eray)=Tcout;
MATRIX_Tcin(eray)=Tcin;
MATRIX_wnet(eray)=wnet;
MATRIX_ncycle(eray)=ncycle;
MATRIX_qin(eray)=qin;
MATRIX_plow(eray)=pp(1)/101.325;
MATRIX_phigh(eray)=pp(2)/101.325;
MATRIX_Tlow(eray)=Tlow;
NESTA=[MATRIX_Tcin;MATRIX_Tcout;MATRIX_wnet;MATRIX_ncycle;MATRI
X_qin;MATRIX_plow;MATRIX_Tlow;MATRIX_phigh];
end
```

REFERENCES

1. CSP World: World news about concentrated solar power. [Online] [Cited: 28 September 2012.] http://www.csp-world.com/resources/4-csp-facts-figures.

2. **Rauf, S. Bobby .** *Thermodynamics made simple for energy engineers.* Lilburn : Fairmont Press, 2012. 0881736503.

3. *A proposed stack configuration for dry cooling tower to improve cooling efficiency under crosswind.* **Goodarzi, M.** 2010, Journal of Wind Engineering and Industrial Aerodynamics, pp. 858-863.

4. **Maulbetsch, John S. and DiFilippo, Michael N. .** *COST AND VALUE OF WATER USE AT COMBINED-CYCLE POWER PLANTS.* s.l. : California Energy Commission, 2006.

5. **Orosz, Matthew S. , et al.** *SMALL SCALE SOLAR ORC SYSTEM FOR DISTRIBUTED POWER.*

6. *Design and testing of the Organic Rankine Cycle.* **Yamamoto, Takahisa, et al.** 26, s.l. : Energy, 2001, pp. 239–251.

7. *Prediction of Evaporation Losses in Wet Cooling Towers.* **Qureshi, Bilal Ahmed and Zubair, Syed M.** 9, s.l. : Heat Transfer Engineering, 2006, Vol. 27, pp. 86–92. 10.1080/01457630600846372.

8. **Maulbetsch, J. S.** *Comparison of Alternate Cooling Technologies for California Power Plants: Economic, Environmental and Other Tradeoffs.* s.l. : CALIFORNIA ENERGY COMMISSION, 2002. 500-02-079F.

9. **Kroger, Detlev G.** *Air-Cooled Heat Exchangers And Cooling Towers: Thermal-Flow Performance Evaluation And Design.* Oklahoma : Pennwell Corp, 2004.

10. **Electric Power Research Institute.** *Comparison of Alternate Cooling Technologies for California Power Plants: Economic, Environmental and Other Tradeoffs.* s.l. : CALIFORNIA ENERGY COMMISSION, 2002.

11. *Improving cooling efficiency of dry cooling towers under cross-wind conditions by using wind-break methods.* **Zhai, Z. and Fu, S.** 2006, Applied Thermal Engineering, pp. 1008-1017.

12. *Effect of cross-flow on the performance of air-cooled heat exchanger fans.* **Stinnes, W. H. and Backström, T. W. von.** 22, s.l. : Applied Thermal Engineering, 2002, pp. 1403–1415.

13. *Measures against the adverse impact of natural wind on air-cooled condensers in power plant.* **LiJun, Yang, XiaoZe, Du and YongPing, Yang.** 53, s.l. : SCIENCE CHINA Technological Sciences, 2010, pp. 1320–1327.

14. *Air-cooled heat exchanger inlet flow losses.* **Meyer, C. J. and Kröger, D. G.** 21, s.l. : Applied Thermal Engineering, 2001, pp. 771-786.

15. *EFFECT OF INLET FLOW DISTORTIONS ON FAN PERFORMANCE IN FORCED DRAUGHT AIR-COOLED HEAT EXCHANGERS.* **SALTA, C. A. and KRÖGER, D. G.** 6, s.l. : Heat Recovery Systems & CHP, 1995, Vol. 15, pp. 555-561.

16. *FLOW DISTORTIONS AT THE FAN INLET OF FORCED-DRAUGHT AIR-COOLED HEAT EXCHANGERS.* **Duvenhage, K., et al.** 1996, Applied Thermal Engineering, Vol. 16, pp. 741-752.

17. *Improving Air-Cooled Condenser Performance in Combined Cycle Power Plants.* **Gadhamshetty, V., et al.** 2006, Journal of Energy Engineering, pp. 81-88.

18. *An estimation of the performance limits and improvement of dry cooling on through solar thermal plants.* **Deng, Huifang and Boehm, Robert F.** 2010, Applied Energy, pp. 216-223.

19. **Kelly, B.** *Nexant Parabolic Trough Solar Power Plant Systems Analysis - Task 2: Comparison of Wet and Dry Rankine Cycle Heat Rejection.* San Francisco, California : National Renewable Energy Laboratory, 2005.

20. **EPRI.** *Comparison of Alternate Cooling Technologies for U. S. Power Plants: Economic, Environmental and Other Tradeoffs.* Palo Alto, California : EPRI, 2004. 1005358.

21. *Design and testing of the Organic Rankine Cycle.* **Yamamoto , Takahisa, et al.** 26, 2001, Energy, pp. 239–251.

22. *Effect of working fluids on organic Rankine cycle for waste heat recovery.* **Liu, Bo-Tau, Chien, Kuo-Hsiang and Wang, Chi-Chuan .** 29, 2004, Energy, pp. 1207–1217.

23. *Energetic and exergetic investigation of an organic Rankine cycle at different heat source temperatures.* **Li, Jing, et al.** 38, 2012, Energy, pp. 85-95.

24. *Operation optimization of an organic rankine cycle (ORC) heat recovery power plant.* **Sun, Jian and Li, Wenhua.** 2011, Applied Thermal Engineering, Vol. 31, pp. 2032-2041.

25. *Numerical analysis of an organic Rankine cycle under steady and variable heat input.* **Bamgbopa, Musbaudeen O. and Uzgoren, Eray.** 107, s.l. : Applied Energy, 2013, pp. 219–228.

26. **Erens, Paul J.** N4 Cooling Towers. *VDI Heat Atlas.* Second Edition. s.l. : Springer Berlin Heidelberg, 2010.

27. *Knowledge base for the systematic design of wet cooling towers. Part I: Selection and tower characteristics.* **Mohiuddin, A. K.M. and Kant, K.** 1, January 1996, International Journal of Refrigeration, Vol. 19, pp. 43-51. 0140-7007.

28. **Coolerado Corporation.** *Coolerado-THE MOST EFFICIENT AIR CONDITIONERS MADE.* [Online] [Cited: 5 May 2012.] http://www.coolerado.com/pdfs/CooleradoHMXPerformanceSI.pdf.

29. **Brill, David J.** Circulating Water Systems. [book auth.] Lawrence F. Drbal, et al. *Power Plant Engineering.* New York : Springer, 1995.

30. **ASHRAE.** *2009 ASHRAE Handbook - Fundamentals (I-P Edition).* s.l. : American Society of Heating, Refrigerating and Air-Conditioning Engineers, Inc., 2009. 978-1933742540.

31. *An Improved Design and Rating Analyses of Counter Flow Wet Cooling Towers.* **Khan, Jameel-ur-Rehman and Zubair, Syed M.** 4, s.l. : Journal of Heat Transfer , 2001, Vol. 123.

32. **Raju, K. S. N. .** *Fluid mechanics, heat transfer, and mass transfer : chemical engineering practice.* Hoboken, N.J. : Wiley, 2011. 9780470637746.

33. **Jones, W. P.** *Air Conditioning Engineering.* 5. Oxford : Butterworth-Heinemann, 2001. pp. 311-325. 9780750650748.

34. *Knowledge base for the systematic design of wet cooling towers. Part II: Fill and other design parameters.* **Mohiuddin, A. K.M. and Kant, K.** 1, s.l. : International Journal of Refrigeration, January 1996, Vol. 19, pp. 52-60. 0140-7007.

35. **Pacific Northwest National Laboratory (PNNL).** *Cooling Towers: Understanding Key Components of Cooling Towers and How to Improve Water Efficiency.* s.l. : U.S. DOE-Federal Energy Management Program, 2011.

36. **Kays, W. M. and London, A. L.** *Compact Heat Exchangers.* Florida : Krieger Pub Co., 1998.

37. **Incropera, Frank P., et al.** *Fundamentals of Heat and Mass Transfer.* 6. Hoboken, NJ : John Wiley, 2007. 978-0470055540.

38. **Kuppan, T.** *Heat Exchanger Design Handbook.* s.l. : CRC Press, 2000. 978-0824797874.

39. **Kakaç, Sadık and Liu, Hongtan.** *Heat Exchangers: Selection, Rating and Thermal Design.* s.l. : CRC PRESS, 2002.

40. **Hesselgreaves, John E.** *Compact heat exchangers : selection, design, and operation.* Amsterdam ; New York : Pergamon, 2001. 9780080428390.

41. **Ghiaasiaan, Mostafa.** *Convective heat and mass transfer.* Cambridge ; New York : Cambridge University Press, 2011. 9781107003507.

42. **Serth, R. W.** *Process heat transfer : principles and applications.* London : Elsevier Academic Press, 2007. 0123735882.

43. **EPRI.** *Water & Sustainability (Volume 3): U.S. Water Consumption for Power Production- The Next Half Century.* March 2002. 1006786.